THESIS – TM185400

RECONFIGURATION OF CABLE-DRIVEN PARALLEL ROBOT BASED ON MOBILE BASE POSITION

RIZAL MUNTASHIR
6007201048

Supervisor
Latifah Nurahmi S.T., M.Sc., Ph.D.

Mechanical Engineering Department
Faculty of Industrial and Systems Engineering
Institut Teknologi Sepuluh Nopember
2022

(This page is empty)

THESIS – TM185400

RECONFIGURATION OF CABLE-DRIVEN PARALLEL ROBOT BASED ON MOBILE BASE POSITION

RIZAL MUNTASHIR
6007201048

Supervisor
Latifah Nurahmi S.T., M.Sc., Ph.D.

Mechanical Engineering Department
Faculty of Industrial and Systems Engineering
Institut Teknologi Sepuluh Nopember
2022

(This page is empty)

TESIS – TM185400

REKONFIGURASI *CABLE-DRIVEN PARALLEL ROBOT* BERBASIS POSISI *MOBILE BASE*

RIZAL MUNTASHIR
6007201048

Dosen Pembimbing
Latifah Nurahmi S.T., M.Sc., Ph.D.

Departemen Teknik Mesin
Fakultas Teknologi Industri dan Rekayasa Sistem
Institut Teknologi Sepuluh Nopember
2022

(This page is empty)

LEMBAR PENGESAHAN TESIS

Tesis disusun untuk memenuhi salah satu syarat memperoleh gelar

Magister Teknik (MT)

di

Institut Teknologi Sepuluh Nopember

Oleh:

RIZAL MUNTASHIR

NRP: 6007201048

Tanggal Ujian: 18 Juli 2022

Periode Wisuda: September 2022

Disetujui oleh:

Pembimbing:

1. Latifah Nurahmi, S.T., M.Sc., Ph.D.
   NIP: 198611162020122012 .....

Penguji:

1. Dr. Eng. Unggul Wasiwitono, S.T., M.Eng.Sc.
   NIP. 197805102001121001 .....

2. Arif Wahjudi, S.T., M.T., Ph.D.
   NIP. 197303222001121001 .....

Kepala Departemen Teknik Mesin
Fakultas Teknologi Industri dan Rekayasa Sistem

Dr. Ir. Atok Setiyawan, M.Eng.Sc
NIP: 196604021989031002

RECONFIGURATION OF CABLE DRIVEN PARALLEL ROBOT BASED ON MOBILE ROBOT POSITION

By : Rizal Muntashir

Student Identity Number : 6007201048

Supervisor : Latifah Nurahmi, ST., M.Sc., Ph.D

ABSTRACT

This research studies reconfiguration scenarios of cable driven parallel robot with three mobile bases. The position of three mobile bases can be reconfigured to move back-and-forth. Dynamic equilibrium of the robot is initially derived. A fifth-degree polynomial is used to generate trajectory which should be followed by the end-effector. During executing a task, the end-effector may tip over due to high cable tension which leads to the loss of wheel reaction forces. To avoid this problem, a concept of Zero Moment Point is applied to maintain robot stability via mobile base reconfiguration. By changing the mobile base position, cable tension can also be reduced which eventually reduce the possibility of tip over. Computational results are provided to show the significant impact of reconfiguration to robot stability. Control design and experiment will be the subject of future research.

Keywords: - *Disaster Robot, Cable Driven Parallel Robot, Reconfigurable, Mobile base position.*

(This page is empty)

TABLE OF CONTENTS

ABSTRACT ..... **i**

TABLE OF CONTENTS ..... **iii**

LIST OF FIGURES ..... **v**

LIST OF TABLES ..... **vii**

ACKNOWLEDGEMENTS ..... **ix**

CHAPTER 1 INTRODUCTION **1**

1.1 Background 1

1.2 Problem Statement 3

1.3 Objectives 3

1.4 Scopes and Limitations 3

CHAPTER 2 LITERATURE REVIEW **5**

2.1 State of The Art 5

2.1.1 Serial and Parallel Manipulators 5

2.1.2 Cable Robots 7

2.2 Theoretical Background 13

2.2.1 Geometric Parameter of a Cable-Driven Parallel Manipulator 13

2.2.2 Kinematic Modeling of Cable-Driven Robot 14

2.2.3 Static Equilibrium 16

2.2.4 Dynamic Equilibrium 16

2.2.5 Control System 17

2.2.6 Iterative Method 18

CHAPTER 3 METHODOLOGY **21**

3.1 Research Flowchart 21

3.2 Robot Dimension 22

3.3 Mathematical Analysis 23

3.3.1 Geometric Analysis 24

3.3.2 Trajectory Generation 25

3.3.3 Kinematic Model 28

3.3.4 Static Analysis 29
3.3.5 Dynamic Analysis 32
3.4 Zero Moment Point (ZMP) of Mobile Base 33
3.4.1 ZMP Tipping 34
3.5 Control Scheme 35
3.6 PI Tuning 37
3.7 Software and Hardware 37
3.8 Comparison of Theoretical and Experimental Results 38
3.8.1 One-Sample t-Test 39
CHAPTER 4 RESULTS AND DISCUSSION 41
4.1 Wrench Feasible Workspace 41
4.2 PI Tuning 42
4.3 Non-Reconfiguration 43
4.3.1 Theoretical Results 43
4.3.2 Experimental Results 46
4.4 Reconfiguration Case I: Tension Minimization 48
4.4.1 Theoretical Results 49
4.4.2 Experimental Results 52
4.5 Reconfiguration Case II: ρ Optimization 60
4.5.1 Theoretical Results 61
4.5.2 Experimental Results 63
CHAPTER 5 CONCLUSIONS AND FUTURE WORKS 73
5.1 Conclusions 73
5.2 Future Works 74
REFERENCES 75

LIST OF FIGURES

Figure 2.1 Open and Closed Kinematics Chains (Marlet, 2006) 6
Figure 2.2 SkyCam is being used to broadcast a Washington Huskies football game in Seattle (Sen Qian, 2018) 7
Figure 2.3 (a) The NIST ROBOCRANE prototype (Albus et Al., 1992) (b) ROBOCRANE for aircraft painting and maintenance (Bostelman et al., 1994) 8
Figure 2.4 Application of CDPR in shipbuilding industry (Bostelman et al., 1999) 9
Figure 2.5 Application of CDPR in large spherical radio telescope (Duan et al., 1999) 9
Figure 2.6 The CoGiRo and The ReelAx8 (Lamaury and Gouttefarde,2013)..... 10
Figure 2.7 IPAnema 1 and IPAnema 2 10
Figure 2.8 Prototype of Sophia-3 (Damiano Zanotto et al., 2014) 11
Figure 2.9 FASTKIT prototype (Pedemonte et al., 2020) 12
Figure 2.10 CDPR prototype (Hor Tan et al., 2021)..... 13
Figure 2.11 Geometric description of a fixed frame CDPR (XueJun Jin et al., 2018) 14
Figure 2.12 Three-DoF cable robot (Gosselin, 2013)..... 15
Figure 2.13 Suspended cable robot with reconfigurable pulley mechanism (Adlina et al. 2020)..... 17
Figure 2.14 Closed-loop position control of the DC motor using PID controller (Maung et al., 2018)..... 18
Figure 3.1 Research Flowchart 21
Figure 3.2 Robot Dimension..... 22
Figure 3.3 Mathematical Analysis Flowchart 23
Figure 3.4 Structure of CDPR on mobile cranes 24
Figure 3.5 Given trajectory for the end-effector 27
Figure 3.6 Geometric properties of CDPR on mobile crane..... 28
Figure 3.7 Free body diagram of end-effector *P*..... 30
Figure 3.8 Free body diagram of mobile base..... 31

Figure 3.9 The Non-reconfiguration control scheme 35
Figure 3.10 Reconfiguration Control Scheme 36
Figure 4.1 Wrench Feasible Workspace 41
Figure 4.2 Tip-Free Wrench Feasible Workspace 41
Figure 4.3 Non-Reconfiguration Trajectory Planning 43
Figure 4.4 Non-Reconfiguration Cable Tension 44
Figure 4.5 ZMP Tipping of Payload 1 kg 45
Figure 4.6 ZMP of Payload 1.3 kg 45
Figure 4.7 Cable Length li of payload 1 kg 46
Figure 4.8 Cable Length li of Payload 1.3 kg 47
Figure 4.9 Trajectory Planning 49
Figure 4.10 The change of ρ of each mobile base 50
Figure 4.11 Cable Tension on Each Cable 50
Figure 4.12 ZMP of Reconfiguration Case I 51
Figure 4.13 Cable Length of Reconfiguration Case I 52
Figure 4.14 Rho in Reconfiguration Case I 53
Figure 4.15 ρ value in Reconfiguration Case II 61
Figure 4.16 Reconfiguration Case II: Cable Tension τ 62
Figure 4.17 ZMP Reconfiguration Case 2 63
Figure 4.18 Cable Length of Reconfiguration Case II 63
Figure 4.19 ρ in Reconfiguration Case II 65

LIST OF TABLES

Table 3.1 Robot Dimension 22
Table 3.2 Boundary Condition of Given Trajectory 27
Table 3.3 Motor Specifications 38
Table 3.4 Boundary Condition of Maximum Error of Cable Length 38
Table 3.5 Boundary Condition of Maximum Error of ρi 39
Table 4.1 Existing Gain 42
Table 4.2 Calibrated Gain for Each Motor 43
Table 4.3 Non-Reconfiguration: Maximum Cable Tension 44
Table 4.4 Maximum Error of Cable Length 47
Table 4.5 Mobile Base Position Reconfiguration Boundary Condition 49
Table 4.6 Reconfiguration Case I Maximum Cable Tension 51
Table 4.7 Reconfiguration Case I: Maximum Error of Cable Length 53
Table 4.8 Reconfiguration Case I: Maximum Error of ρ 54
Table 4.9 Reconfiguration Case I: Theoretical and Experimental Results of Cable Length For $l1$ 54
Table 4.10 Reconfiguration Case I: P-Value from One-Sample t-Test of Cable Length For $l1$ 55
Table 4.11 Reconfiguration Case I: Theoretical and Experimental Results of Cable Length For $l2$ 55
Table 4.12 Reconfiguration Case I: P-Value from One-Sample t-Test of Cable Length For $l2$ 56
Table 4.13 Reconfiguration Case I: Theoretical and Experimental Results of Cable Length For $l3$ 56
Table 4.14 Reconfiguration Case I: P-Value from One-Sample t-Test of Cable Length For $l3$ 57
Table 4.15 Reconfiguration Case I: Theoretical and Experimental Results of $\rho 1$ 57
Table 4.16 Reconfiguration Case I: P-Value from One-Sample t-Test of $\rho 1$ 58
Table 4.17 Reconfiguration Case I: Theoretical and Experimental Results of $\rho 2$ 58
Table 4.18 Reconfiguration Case I: P-Value from One-Sample t-Test of $\rho 2$ 59

Table 4.19 Reconfiguration Case I: Theoretical and Experimental Results of $\rho 3$ 59
Table 4.20 Reconfiguration Case I: P-Value from One-Sample t-Test of $\rho 3$ 59
Table 4.21 Reconfiguration Case II Maximum Cable Tension 62
Table 4.22 Maximum Error of cable Length in Reconfiguration Case II 64
Table 4.23 Maximum Error of ρ 65
Table 4.24 Reconfiguration Case II: Theoretical and Experimental Results of Cable Length For $l1$ 66
Table 4.25 Reconfiguration Case II: P-Value from One-Sample t-Test of Cable Length $l1$ 66
Table 4.26 Reconfiguration Case II: Theoretical and Experimental Results of Cable Length For $l2$ 67
Table 4.27 Reconfiguration Case II: P-Value from One-Sample t-Test of Cable Length $l2$ 67
Table 4.28 Reconfiguration Case II: Theoretical and Experimental Results of Cable Length For $l3$ 68
Table 4.29 Reconfiguration Case II: P-Value from One-Sample t-Test of Cable Length $l3$ 68
Table 4.30 Reconfiguration Case II: Theoretical and Experimental Results of $\rho 1$ 69
Table 4.31 Reconfiguration Case II: P-Value from One-Sample t-Test of $\rho 1$ 69
Table 4.32 Reconfiguration Case II: Theoretical and Experimental Results of $\rho 2$ 70
Table 4.33 Reconfiguration Case I: P-Value from One-Sample t-Test of $\rho 2$ 70
Table 4.34 Reconfiguration Case II: Theoretical and Experimental Results of $\rho 3$ 70
Table 4.35 Reconfiguration Case II: P-Value from One-Sample t-Test of $\rho 3$ 71

ACKNOWLEDGEMENTS

First of all, I would like to express my highest gratitude to Allah SWT for blessing, love, and knowledge so that I could finish this thesis. In this valuable chance, I would gratefully acknowledge and appreciate a number of people for their help and support for this thesis.

My first and sincere appreciation goes to my thesis supervisor, **Latifah Nurahmi., S.T., M.Sc., Ph.D** for her marvelous supervision, guidance, and encouragement. Sincere gratitude is extended to her genereous participation in guiding, constructive feedback, kind advice during my master program.

I would extend my infinite appreciation to the love of my life, my mom, **Dra. Hidayati Prihartini**, for her advice, encouragement and absolute patience for having me as her son. Without her love and support, I would not be in the place where I am right now. Sense of respect goes to my father, **Hewin Setyowinarko**, who financially support me during my master program.

Moreover, I gratefully recognize the help from my predecessors, **Hor Tan and Dimas**, who helped me with the simulation and analysis. I am also thankful to all control system engineering lab members, **Billy, Khafid, Candra, and Uyab** who help me through the hard times. I am fortunate to have been part of RSK lab. I thank **Tim Hore** for the relentless support and encouragement. I would also mention **Yayang, Eko, and Faiz** who also supported me since the bachelor program. I would also thank my SMADA friends, **Iqbal, Iqbaal, Claresta, Rere, El, Dhia, and Piyo** who accompanied me since the high school. Sense of gratitude goes to **Shafiyah Salsabila, S.T** for helping me with the translation and her undeniable support.

Furthermore, I would like to extend my gratitude to my Achmari family, specially to my cousins who never stop praying and caring for me. Thank you all.

(This page is empty)

CHAPTER 1
INTRODUCTION

Parallel robot is commonly known as robots that has closed kinematic chains, which means there are at least two actuators meet as an end-effector. Cable-driven parallel robot is a type of parallel robots whose end effector hold up in parallel by several cables whose tension are controlled by actuators. The motion of an end effector can be controlled by changing the length of the cables continuously and relocating the position of the mobile base continuously.

The concepts and ideas of the cable-driven parallel robots were first introduced in the late 1980s. Owing to unique properties of the robots, such as the immense size of the workspace, the possible amount of payload that could be lifted, and the dynamic abilities, the potential utility became obvious and successful application seemed feasible.

1.1 Background

Located at the confluence of four tectonic plates, Indonesia is an archipelago prone to disasters such as volcanic eruptions, earthquakes, tsunamis, floods and landslides. Moreover, Indonesia is located in the circum-pacific belt, commonly known as the Ring of Fire, a 40.000 km basin that is associated with continuous series of oceanic trenches, volcanic arcs, and volcanic belts. Indonesia is named as one of the countries that have a high level of seismicity in the world, more than ten times the level of seismicity in the United States (Arnold,1986). There is also a climate condition in Indonesia that can cause some bad consequences such as the occurrence of hydrometeorological disasters such as floods, landslides, forest fires and drought.

A primordial task for fire and rescue services is to search for possible human survivors on the disaster site. Due to the uncertain condition on the incident cite, the task to search and rescue become complex and high-risk, which can lead to loss of lives among the crisis managers themselves. Time is the most critical factor for

the search and rescue process, as the survival rate of the victims or the survivors decreases rapidly. The evacuation process in any disaster cite in the world is too often time consuming. It may take days, weeks, or even months. The introduction of Cable-driven parallel robot could offer a valuable tool to save human lives and to speed up the evacuation process.

Cable-driven parallel robots (CDPRs) are essentially robots that have a movable mobile platform connected to an amount of cables that driven by actuators supported on each base frame. Numerous research studies have been conducted to determine the conditions for obtaining workspace, stiffness and singularities. The application of cables allows CDPRs having unique properties such as a potentially very large workspace, large payload-to-weight ratio, and high dynamics capabilities. The moving platform is moved by changing the cable lengths those are connected to the base. The large of the workspace could become larger if the robots are set to be reconfigurable, an ability that allows CDPRs change their geometric structure. CDPRs with a reconfigurable ability are widely known as Reconfigurable Cable-Driven Parallel Robots.

The reconfiguration existed are too often discrete and run manually. To attain the imposed requirement concerning the interference free cable circulation, a concept of Mobile Cable-Driven Parallel Robots (MCDPRs) is introduced. FASTKIT has been introduced as the first autonomous and deployable prototype of MCDPRs. The use of the mobile base allows the robots having a larger workspace, since in mechanical point of view, it is relatively easy to change the geometry of the CDPRs by modifying the location of the winches exit points or by changing the location of the cable attachment points on the load. The concept mobile crane robot applies the same circumstance as the MCDPRs.

1.2 Problem Statement

The problems to be addressed through this research are:

1. How is the static and dynamic analysis of the robot?
2. How to control the reconfiguration of the robot based on the mobile base position?
3. What is the result from the experiment?

1.3 Objectives

The aim of this study is to design and implement a reconfiguration of the mobile crane based on its position. The objectives outlined to achieve this aim are:

1. To provide static and dynamic analysis of the robot
2. To provide a control design of reconfiguration of the robot based on the mobile base position
3. To perform an experiment and analyze the experimental results.

1.4 Scopes and Limitations

The scope of this research focuses on:

1. Static and dynamic analysis of a mobile crane and its point mass
2. The end-effector is considered as point mass.
3. The mobile bases positions are controlled as the reconfiguration
4. The height of each crane is set to be fixed

(This page is empty)

CHAPTER 2
LITERATURE REVIEW

Historically, mankind has continue developing progressively sophisticated mechanism and machines for various uses and tasks, including moving specific objects with respect to a fixed or mobile base. The term *robot* or *manipulator* applies in every mechanical system that can move objects with respect to its base and able to control two or more degrees of freedom. Over the last decade, scientific and technological developments in both theoretical and practical allowed robotic devices to massively expand their application. This chapter presents a review of previous research, theoretical background, and how they relate to the current study.

2.1 State of The Art

The scientific community across the world has shown interest in emerging issues from robot development. Due to the immense development, robotic manipulator has shown its huge contribution in replacing human for completing industrial repetitive operations in assembly or manufacturing lines, some high-risk tasks such as disaster robots, and some unhealthy tasks such as welding and painting.

2.1.1 Serial and Parallel Manipulators

Robotic manipulators are primarily classified based on the structure of the robots. Robots whose structure is replicating a human arm, constructed by connecting several rigid bodies with revolute joints, generating one degree of freedom between two translational links as shown in Figure 2.1a. The sequence of linked bodies is known as *open kinematic chain*. Manipulators applying an open kinematic chain structure are called *serial robots*.

Despite of the advantages, such a large workspace compared to their fix based, serial robots with their open chain mechanism are attributed with several drawbacks.

The drawbacks are such as:

- A small payload to robot weight ratio
- Poor positioning accuracy
- Low speed and acceleration

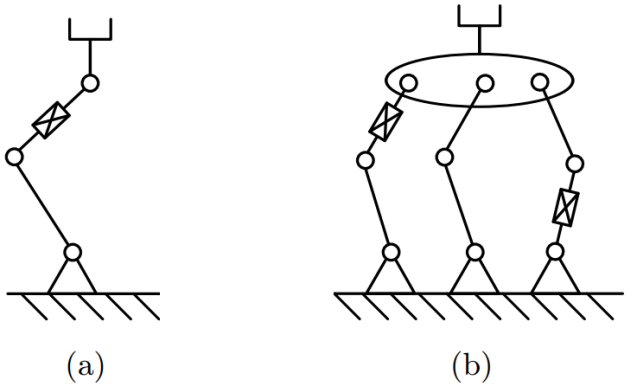

Figure 2.1 Open and Closed Kinematics Chains (Marlet, 2006)

These drawbacks can be solved by adding multiple open kinematic chains whose base connected to the end-effector. By adding several open kinematic chains, it allows the external force distributed to the base. This structure than formed a *closed kinematic chain* mechanism as shown in Figure 2.1b. (Merlet, 2006) defined a closed-loop kinematic chain mechanism whose end-effector is linked to the base by several independent kinematic chains is a *parallel manipulator*.

The advanced development of manufacturing process allows parallel robots having various structures which perform multiple tasks. However, the mechanism of parallel robots with rigid bodies leads the robot having reduced workspace compared to their dimensions. The reduced workspace causes parallel robots having some drawbacks such as

- Restricted motion range
- Limited displacement of the end-effector
- Possible interference between links

2.1.2 Cable Robots

Researchers come out with an idea to replace the rigid body legs with cables in the parallel robots, connecting the robot base to the end-effector. Hence, a parallel robot that applies cables as links is called a *Cable-Driven Parallel Robot* (CDPR). In favor to avoid misconception of the robot that is being discussed in this thesis, the definition of CDPR is as follows:

A *Cable-Driven Parallel Robot* or simply *Cable Robot* is a parallel manipulator whose mobile platform connected to the fixed or mobile platform only by cables and its position is controlled by reconfiguring the lengths of the cables or the position of the fixed or mobile base.

The change of the rigid body legs to the cables allows the robots performing tasks that require larger workspace and larger payload capacity. The use of cables reduces the moving mass significantly, which gives CDPR a lightweight structure. The flexibility of the cables can solve the interference and restricted joint motion problems. Regardless their flexibility, cables can have a high tensile strength with respect to their diameter and their linear density. Additionally, the utility to attach and detach the cables to the end-effector makes the CDPR reconfigurable.

In the mid-1980s August Design Company developed *SkyCam*, a cable-suspended camera system with 4 cables and can move up to 44.8 km/h maximum speed (Sen Qian, 2018). It used widely for live broadcasting in large scale and high-speed tracking photography, as shown in Figure 2.2.

Figure 2.2 SkyCam is being used to broadcast a Washington Huskies football game in Seattle (Sen Qian, 2018)

The National Institute of Standards and Technology (NIST) developed The NIST ROBOCRANE, a robot crane consists of a stable platform supported by six cables suspended from three points on a fixed or mobile octahedral structure, as shown in Figure 2.3a. The ROBOCRANE applies six winches, which are controlled by computer, to control the lengths of the six cables.

(a) (b)

Figure 2.3 (a) The NIST ROBOCRANE prototype (Albus et Al., 1992) (b) ROBOCRANE for aircraft painting and maintenance (Bostelman et al., 1994)

Due to its octahedron structure, The ROBOCRANE has an advantage of high lift-to-weight ratio. The principal application of this robot is to be lifting and positioning objects or power tools weighing up to 1 ton. This robot crane can lift up a payload of 455 kg without no strain on the working winches. It requires no counterweight and experiences neither twisting nor bending moments. Regardless the stand out results, this robot still need a more advanced sensing capability and additional mechanical analysis and testing. (Bostelman et al., 1994) proposed the application of the robot for aircraft painting as shown in Figure 2.3b. It allows the operator to work inside a movable platform and move across the aircraft with less risk of operator stress and injury. (Bostelman et al. 1999) shows the application of ROBOCRANE in shipbuilding industry, where it can be used as a gantry crane to provide more precise control of the welding platform, as shown in Figure 2.4a. Also applied in the shipbuilding industry, the application of ROBOCRANE could be used as a movable suspended scaffolding and provide a much safer operator access to ship as depicted in Figure 2.4b.

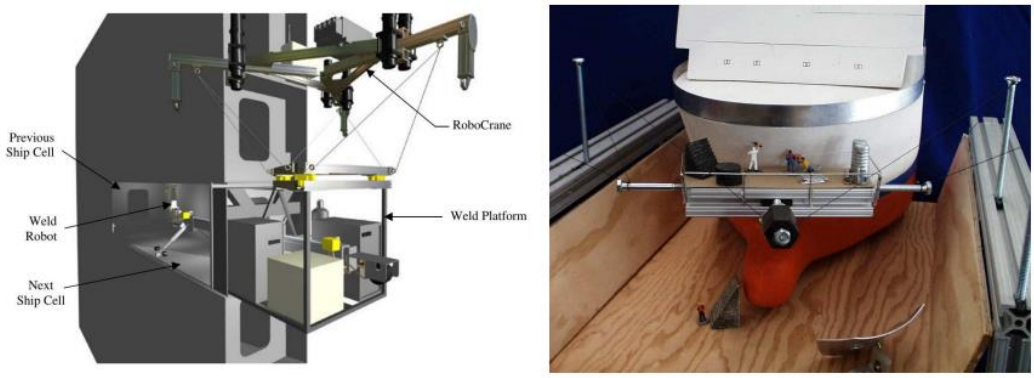

(a) (b)

Figure 2.4 Application of CDPR in shipbuilding industry (Bostelman et al., 1999)

(Duan et al., 1999) initiated an application of CDPR as a feed support system in 500 meters aperture spherical radio telescope (FAST) in China to move the feed platform across the large spherical telescope as shown in Figure 2.5.

Figure 2.5 Application of CDPR in large spherical radio telescope (Duan et al., 1999)

To achieve well-performed design solutions for a given design requirement, (Giulio Rosati et al. 2011) proposed an adaptive design to control a cable-driven system. The term adaptive refers to the capability of modifying in real time the configuration of the cable entry points to maximize the workspace. The device is defined as *fully adaptive* when a complete decoupling between the end-effector

pose and the optimal cable configuration is achieved. The device is *semi-adaptive* when the disposition of the cables can only be kept inside an acceptable set.

Figure 2.6 The CoGiRo and The ReelAx8 (Lamaury and Gouttefarde,2013)

In the last 10 years, CDPRs have become very popular among researchers across the world and numerous publications have been published widely. Several prototypes are capable to perform freight management and pick and place tasks, such as the *CoGiRo* (Lamaury and Gouttefarde, 2013) and the *ReelAx8* (Dallej, 2012) those developed by team Dexter at LIRMM, as shown in Figure 2.6. The Fraunhofer Institute of Stuttgart has developed the IPAnema, a family of cable-diven parallel robots for industrial applications, shown in Figure 2.7.

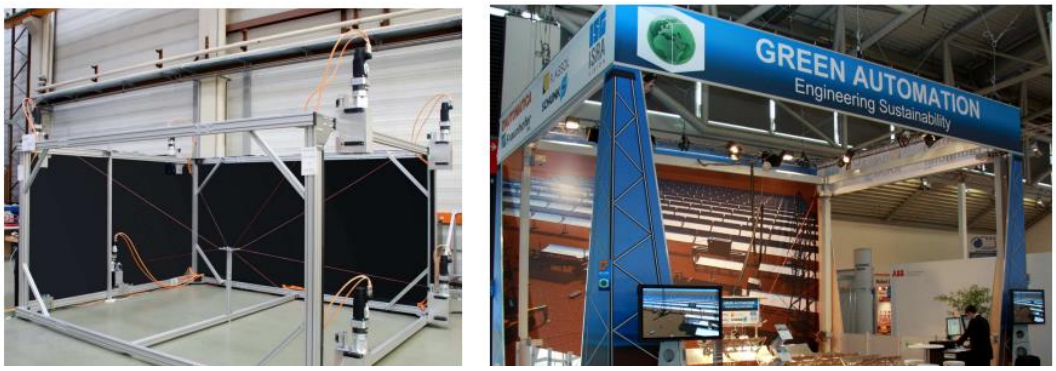

Figure 2.7 IPAnema 1 and IPAnema 2

(Nguyen et al. 2014) has performed an optimization for the reconfiguration of the CDPR by solving a multi-objective optimization problem with non-linear constraints. The power consumption of the robot is quantified by the sum of the cable tension. The reconfiguration solution which minimizes the sum of the cable

tension, the cables tend to be as vertical as possible. On the other hand, by minimizing the normalized upper bound, the cables tend to become horizontal. The use of derivative free algorithm to solve the CDPR reconfiguration may be time consuming thus obtain more reliable solution.

Sophia-3, a post-stroke rehabilitation device developed by (Damiano Zanotto et al., 2014) is a cable-driven device with a tilting working plane as shown in Figure 2.8. It features a moving pulley-block that allows the robot to achieve excellent force capabilities due to its semi-adaptive design would yield the maximum force performance over the whole workspace, despite the low number of cables. Sophia-3 plane, in which the exercise is performed, can be tilted between the horizontal and a maximum tilting angle of 60°. This feature allows Sophia-3 to assist rehabilitation exercises in which the shoulder can be exercised against gravity.

Figure 2.8 Prototype of Sophia-3 (Damiano Zanotto et al., 2014)

The term *Mobile Cable-Driven Parallel Robot* applies when the base of that connected to the CDPR is a mobile base or mobile robot instead of fixed base. Two Mobile CDPRs (MCDPRs) prototype have been developed and have shown stand out results. FASTKIT (Pedemonte et al., 2020) is a mobile cable-driven parallel robot for logistic, shown in Figure 2.9. FASTKIT aims at providing the user with flexible and low-cost logistic solution to equip small warehouses. The novelty of this project lies in the combination of autonomous mobile platforms and a CDPR.

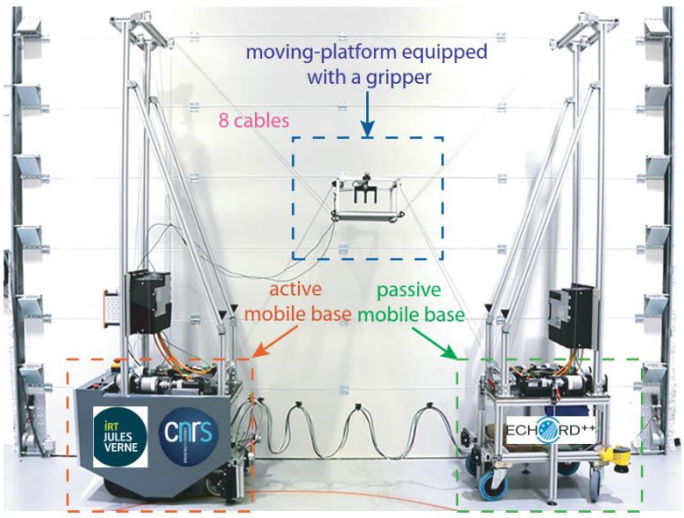

Figure 2.9 FASTKIT prototype (Pedemonte et al., 2020)

FASTKIT is capable of autonomously navigating in its environment to reach the task location referred to as a navigation mode. It should be noted that FASTKIT consists of an active and a passive mobile base carrying a six DoF moving platform which is pulled by 8 cables. The mobile bases are planar robots. Hence, they can only navigate in a plane parallel to the ground.

Hor Tan et. al, 2021 has developed *Reconfigurable* CDPR with multiple cranes as shown in Figure 2.10. Three mobile bases were set fixed at a distance of $\rho_i = 1.5\ m$ from the origin O. Without the reconfiguration of the crane, the end-effector with payload of 1kg, successfully followed the given trajectory. However, when the payload of 1.3kg is applied to the end-effector the system turned unstable and mobile base 3 tipped on the v axis. By ***Reconfigurable*** it means that the CDPR is able to change the locations of its cable exit points, defined as the exit points between the cables and the robot base frame. A change in the configuration of robot's geometry, such as the crane height or the distance of the frame base position to the origin is defined as a ***Reconfiguration***.

Hor Tan proposed two scenarios of reconfigurations. Reconfiguration Case I is the cable tension minimization which meant to minimize the cable tension by

moving up the crane up and downward. In Reconfiguration Case II, the Pareto Optimization is used to optimize the crane height.

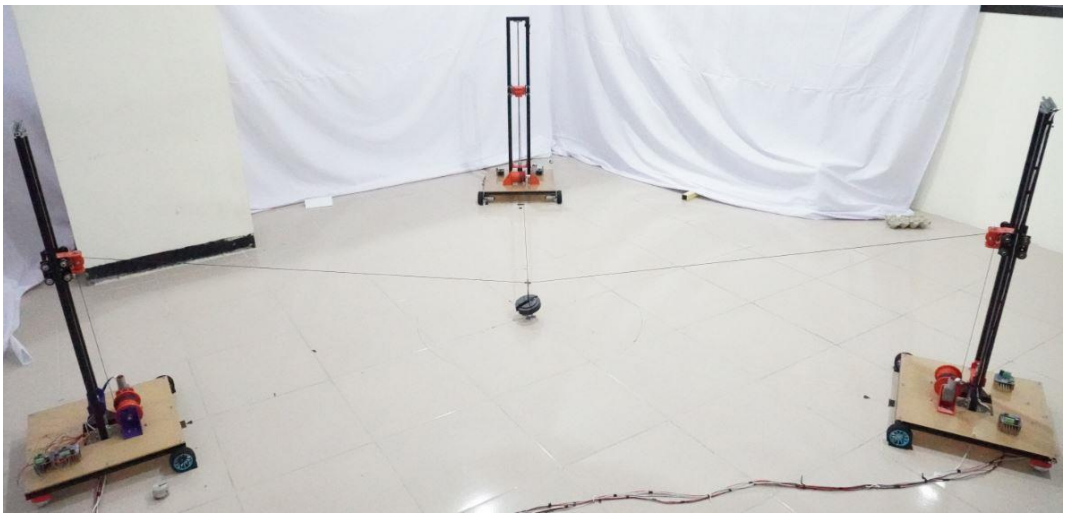

Figure 2.10 CDPR prototype (Hor Tan et al., 2021)

However, the measurement of cable tension did not come from the actual measurement using a tension sensor. The high vibration on the cable might disturb the end-effector to track the given trajectory. The system did not track the actual position of the end-effector using a sensor such IMU or lidar camera.

2.2 Theoretical Background

This chapter provides supporting theories regarding to the research.

2.2.1 Geometric Parameter of a Cable-Driven Parallel Manipulator

The robot end-effector is designed with respect to the generated robot task and positioned within a workspace to fulfill a specific work. The cables are connected to the end-effector and generate six DoF motions. The motors winches control the cable length and tension for a specific task. Generally, to calibrate the kinematic model, the model must include the most significant geometric and non-geometric parameters that influence control accuracy.

The kinematic model of eight-cable driven parallel robot shown in Figure 2.11 is given by:

$$l_i = a_i - x - R_{b_i} \tag{2.1}$$

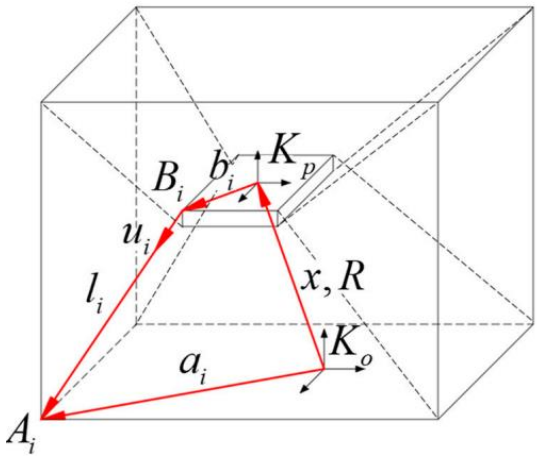

Figure 2.11 Geometric description of a fixed frame CDPR (XueJun Jin et al., 2018)

As shown in Figure 2.11, the geometry of the robot is described by its proximal anchor points or exit points on the robot base A_i and the distal anchor point on the end-effector B_i, which are defined by the vectors a_i and b_i. x and R define the position and orientation of the end-effector fixed frame K_p with respect to the global coordinate K_o. It is clear that all the configuration parameters need to be accurately determined before implementation.

2.2.2 Kinematic Modeling of Cable-Driven Robot

Many cable-suspended parallel mechanisms were designed to work in static or quasi-static equilibrium. The workspace of these devices can be determined based on the static equilibrium of the moving platform. By dynamically controlling the robots, their workspace can be extended beyond the static workspace and the notion of dynamic workspace arises.

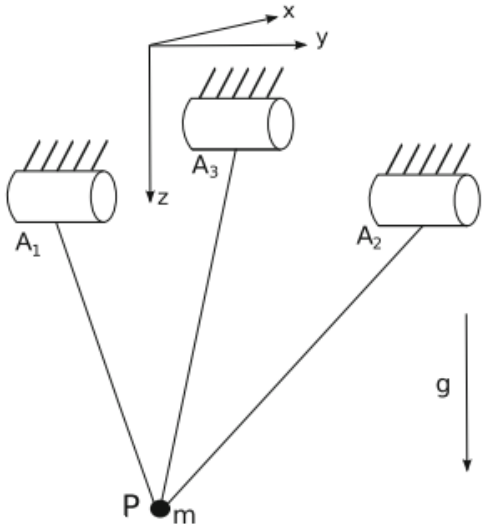

Figure 2.12 Three-DoF cable robot (Gosselin, 2013)

Firstly, a fixed frame is defined on the base of the robot. The Z-axis of the fixed frame is pointing downwards as illustrated in Figure 2.12. In this case, the spools are assumed to be fixed and are noted as A_i, and $i \in 1,2,3$. The vector $\mathbf{a}_i$ is the vector connecting the origin of the fixed frame reference to the A_i. The position of end-effector is noted as $\mathbf{p} = [x, y, z]^T$. The cable length is respectively noted as ρ_i. The inverse kinematic equation then can be written as

$$\rho_i = \sqrt{(\mathbf{p} - \mathbf{a}_i)^T (\mathbf{p} - \mathbf{a}_i)}\,, \qquad i = 1,2,3 \tag{2.2}$$

Then, the unit vectors along the direction of the cables are defined as

$$\mathbf{u}_i = \frac{\mathbf{p} - \mathbf{a}_i}{\|\mathbf{p} - \mathbf{a}_i\|} = \frac{1}{l_i}(\mathbf{p} - \mathbf{a}_i), \qquad i = 1,2,3 \tag{2.3}$$

2.2.3 Static Equilibrium

A six DoF mobile CDPR with 8 cables connected to 4 mobile bases built by (Rasheed et al., 2020) has the static equilibrium equation of the moving platform as follows:

$$\sum_{j=1}^{p}\sum_{i=1}^{m_j}\mathbf{u}_{ij}t_{ij} = \mathbf{f} \tag{2.4}$$

where $\mathbf{f} = [f^x, f^y, f^z]^T$ is denoted as the forces applied by the cables. t_{ij} is the cable tension. The static equilibrium of the moving platform is then expressed in a matrix form as follows:

$$\mathbf{Wt} = \mathbf{w} \tag{2.5}$$

where $\mathbf{W}$ is a wrench matrix mapping the cable tension ($\mathbf{t} \in \mathbb{R}^m$) onto the wrenches ($\mathbf{w} \in \mathbb{R}^n$) applied by the cables onto the moving platform.

$$\mathbf{W} = \left[W_{\mathbf{1}}, \dots W_j \dots W_p\right], \mathbf{w} = \begin{bmatrix}\mathbf{f}\\ \mathbf{m}\end{bmatrix}, \mathbf{t} = \begin{bmatrix}\mathbf{t}_1\\ \vdots\\ \mathbf{t}_j\\ \vdots\\ \mathbf{t}_{\boldsymbol{p}}\end{bmatrix} \tag{2.6}$$

The cable tension t is bounded between a minimum and a maximum tension.

2.2.4 Dynamic Equilibrium

Given a fixed frame CDPR which has 6 DoF and 4 cables connected to an effector. The dynamic analysis aims to define the behavior of the cable robot when certain amount of forces and moments are imposed onto the moving platform (Syamlan, A.T., Nurahmi, L., Tamara, M.N. et al., 2020). The analysis is based on the Newton's law of motion, which can be expressed as:

$$\mathbf{W}\tau + \mathbf{w}_e = m\ddot{\mathbf{p}} \tag{2.7}$$

where $\mathbf{W} = \mathbf{J}^T$ is the wrench matrix, τ is the tension applied on each cable and the external wrench acting on moving platform is noted as $\mathbf{w}_e$. m and $\ddot{\mathbf{p}}$ are the mass and the acceleration of the moving platform.

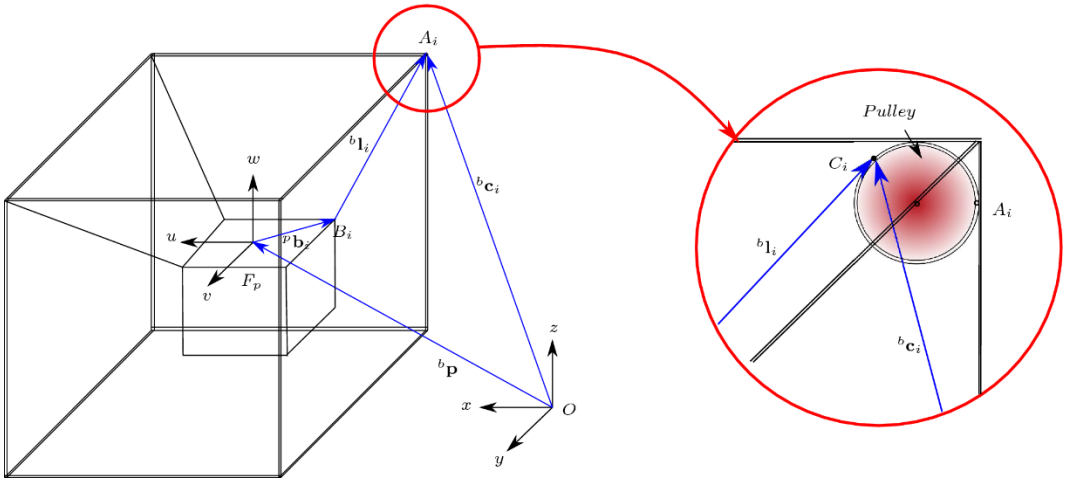

Figure 2.13 Suspended cable robot with reconfigurable pulley mechanism (Adlina et al. 2020)

Figure 2.13 depicts the geometric description of a fixed frame suspended cable robot with 4 cables connected to the end-effector. The geometric center of the moving platform is denoted by point P. The pulley is attached onto each corner of the cube base frame and it is referred as an exit point A_i.

2.2.5 Control System

With its three-term functionality covering treatment to both transient and steady-state responses, proportional-integral-derivative (PID) control offers the simplest and yet most efficient solution to many real-world control problems (Ang, K.H. et al., 2005). Since the invention of PID control in 1910 (largely owning to Elmer Sperry's ship autopilot), and the Ziegler–Nichols' (Z-N) straightforward tuning methods in 1942, the popularity of PID control has grown tremendously.

PID controller is known as the 'three-term' controller which transfer function is generally written in the parallel form or the ideal form which can be expressed as

$$G(s) = K_P + K_I \frac{1}{s} + K_D s = K_P(1 + \frac{1}{T_I s} + T_D s \qquad (2.8)$$

where K_P is the proportional gain, K_I is the integral gain, $K_D$the derivative gain, T_I the integral time constant, and T_D the derivative time constant. The block diagram of PID is illustrated in Figure 2.14

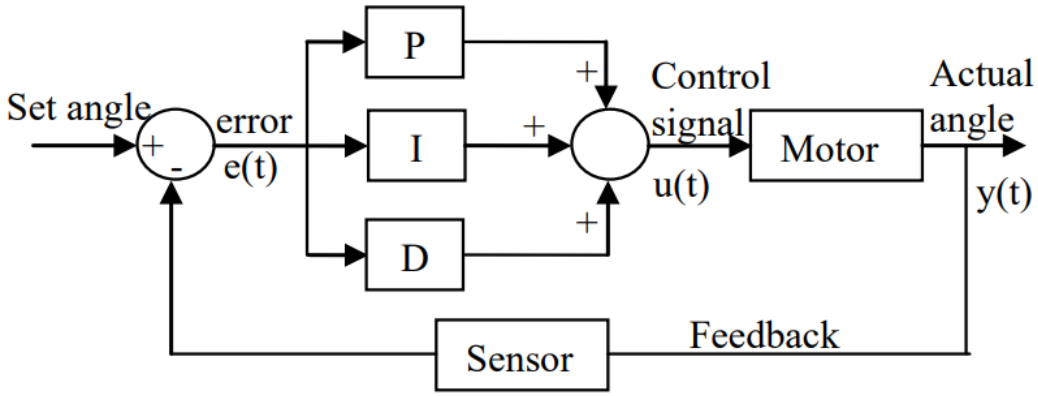

Figure 2.14 Closed-loop position control of the DC motor using PID controller (Maung et al., 2018)

A drawback of feedback control is that an error required before the joint begin to move. It would eb preferable to use our knowledge of the desired trajectory θ_d to initiate motion before any error accumulates.

2.2.6 Iterative Method

Iterative methods produce an approximate solution to the linear system after a finite number of steps. (Studies in Mathematical and Its Applications, p 2004). These methods are useful for large systems of equations where it is reasonable to trade-off precision for a shorter run time. Iterative methods use the coefficient matrix only indirectly, through a matrix-vector product or an abstract linear operator. Iterative methods can be used with any matrix, but they are typically applied to large sparse matrices for which direct solves are slow. The speed of solving a linear system with an indirect method does not depend as strongly on the fill pattern of the coefficient matrix as a direct method. However, using an iterative method typically requires tuning parameters for each specific problem.

Iterative methods are also applied to the computation of approximate solutions of stationary and evolutionary problems associated with differential equations. These methods are based upon certain transformations of differential problems into integral ones. If one can prove that the respective integral operator is subject to the boundary, then all the results of the general theory (existence, convergence, and error estimates) are applicable to the problem considered.

As in example, given the norm

$$\|u\| \coloneqq \max_{t\in[t_0,t_1]} |u(t)| \tag{2.9}$$

Then

$$\begin{aligned} \|T_z - T_y\|, &= \max_{t\in[t_0,t_1]} \left| \int_0^t \varphi\big(s, z(s)\big) - \varphi\big(s, y(s)\big) ds \right| \\ &\leq \max_{t\in[t_0,t_1]} L \int_{t_0}^{t} |z(s) - y(s) ds \leq \max_{t\in[t_0,t_1]} L \int_{t_0}^{t_1} |z(s) - y(s) ds \\ &\leq L(t_1 - t_0) \max_{t\in[t_0,t_1]} |z(s) - y(s)| = L(t_1 - t_0)\|z - y\| \end{aligned} \tag{2.10}$$

We see that if

$$t_1 < t_0 + L^{-1} \tag{2.11}$$

then the operator T is q-contractive if

$$q \coloneqq L(t_1 - t_0) < 1 \tag{2.12}$$

Therefore, if the interval $[t_0, t_1]$ is small enough. Moreover, this solution can be found by the iteration procedure whose accuracy is controlled by estimates.

(This page is empty)

CHAPTER 3
METHODOLOGY

3.1 Research Flowchart

The flowchart methodology of this research is available in the Figure 3.1. This research includes literature review, stating the problems, objectives and limitation, mathematical analysis, designing a control system, doing some study cases, and comparing the theoretical and experimental results.

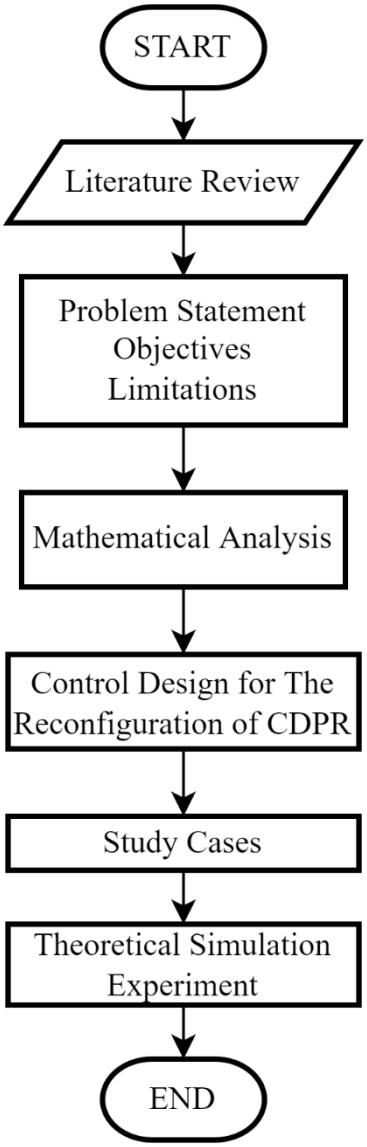

Figure 3.1 Research Flowchart

3.2 Robot Dimension

The dimension of the CDPR is described by Table 3.1 and Figure 3.2.

Table 3.1 Robot Dimension

Properties	Symbol	Value
Length (m)	L	0.35
Width (m)	W	0.45
Crane Length (m)	r_i	0.53-0.83
Crane Mass (kg)	m_I	1.8
Mobile Base Height (m)	b_i^z	0.07
Mobile Base Mass (kg)	m_{II}	3.09
Spool diameter (m)	D	0.06

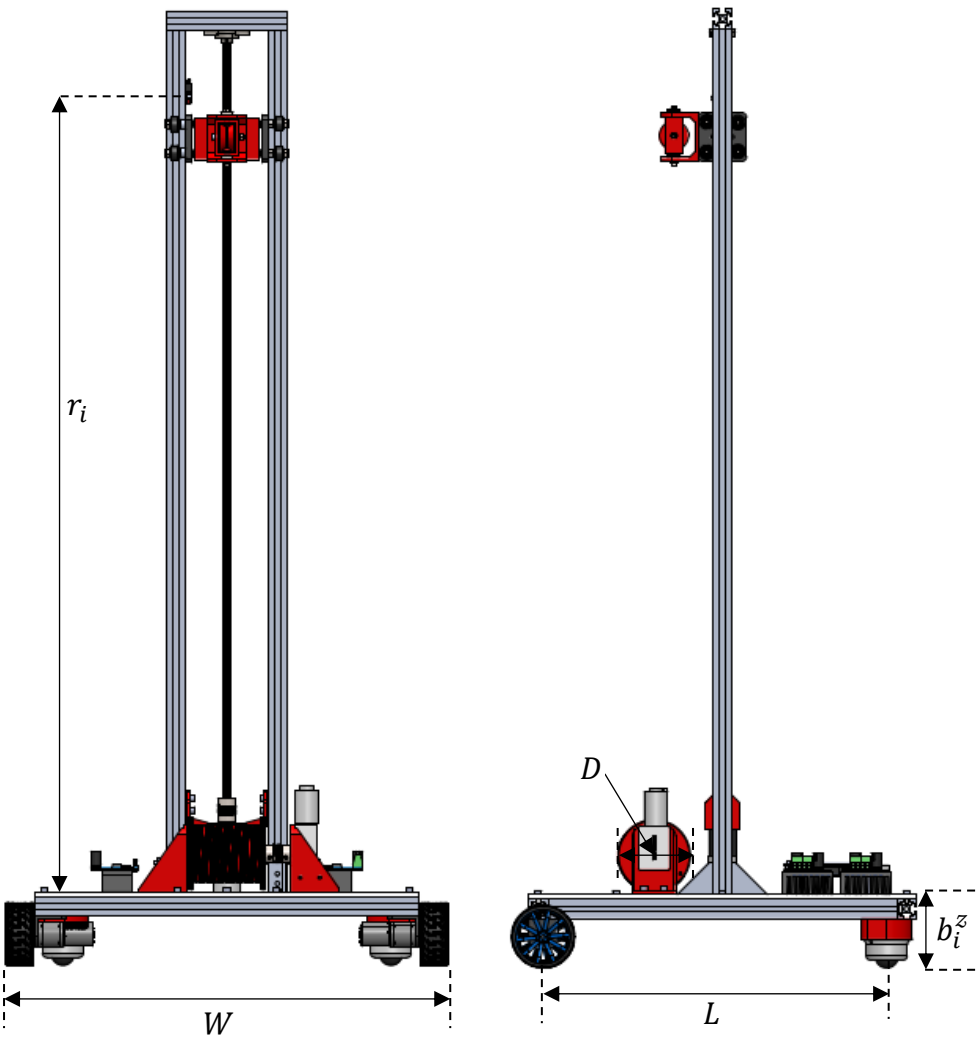

Figure 3.2 Robot Dimension

3.3 Mathematical Analysis

The mathematical analysis that is required for this research is described in a flowchart which is available in the Figure 3.3. As shown in Figure 3.3, the mathematical analysis is started by defining the research parameters and ended by analyzing the zero-moment point.

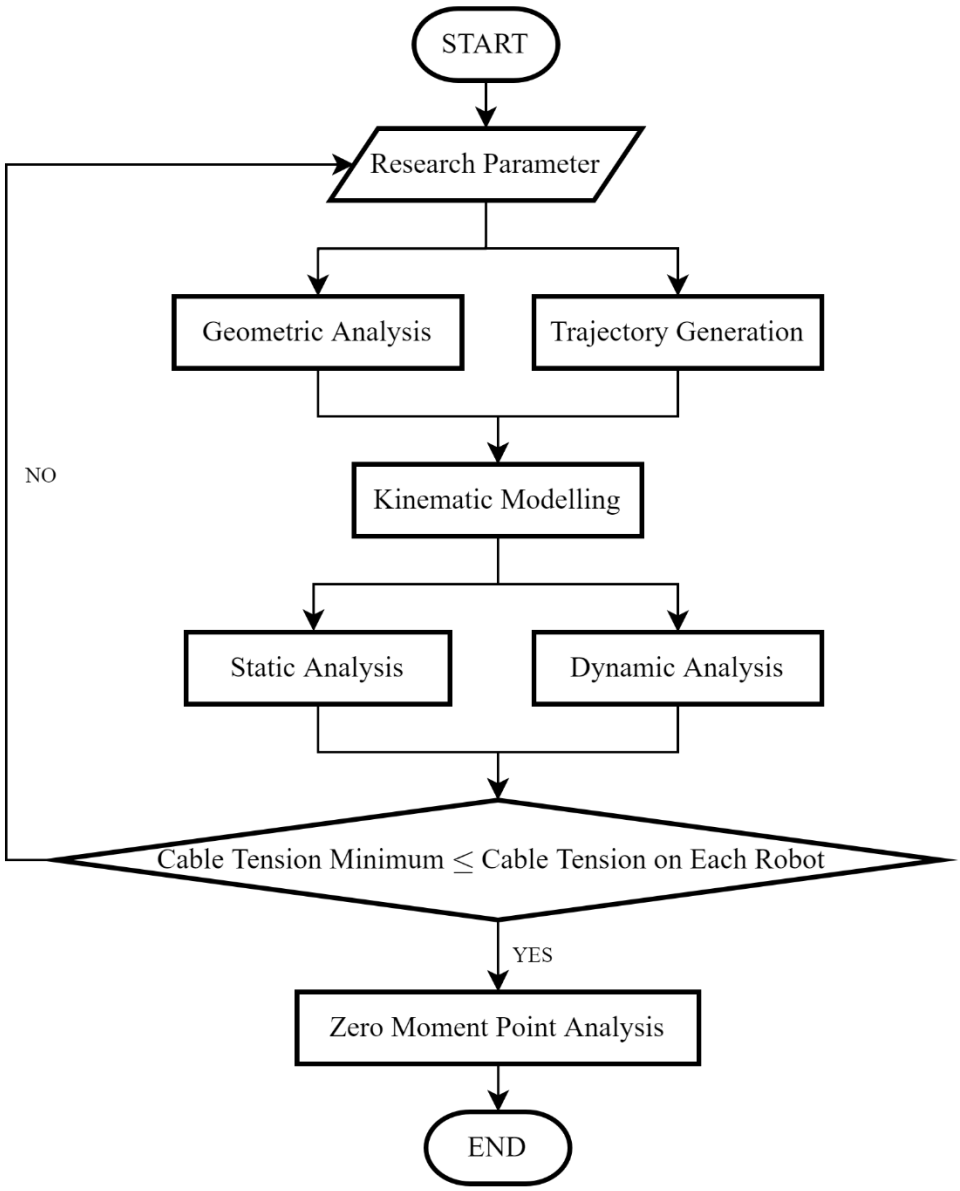

Figure 3.3 Mathematical Analysis Flowchart

3.3.1 Geometric Analysis

The structure of CDPR on the mobile cranes isometric view and its top view are shown in Fig 3.3a. and 3.3b. The local coordinate of three mobile cranes is stated in $\mathcal{L}(o_i, u_i, v_i, w_i)$. Initially, each mobile crane is located at the origin o_i with the distance of ρ_i from the origin O of the fixed coordinate $\mathcal{F}(O, X, Y, Z)$ and the angle γ_i is measured counterclockwise for X-axis as shown in figure 3.3b.

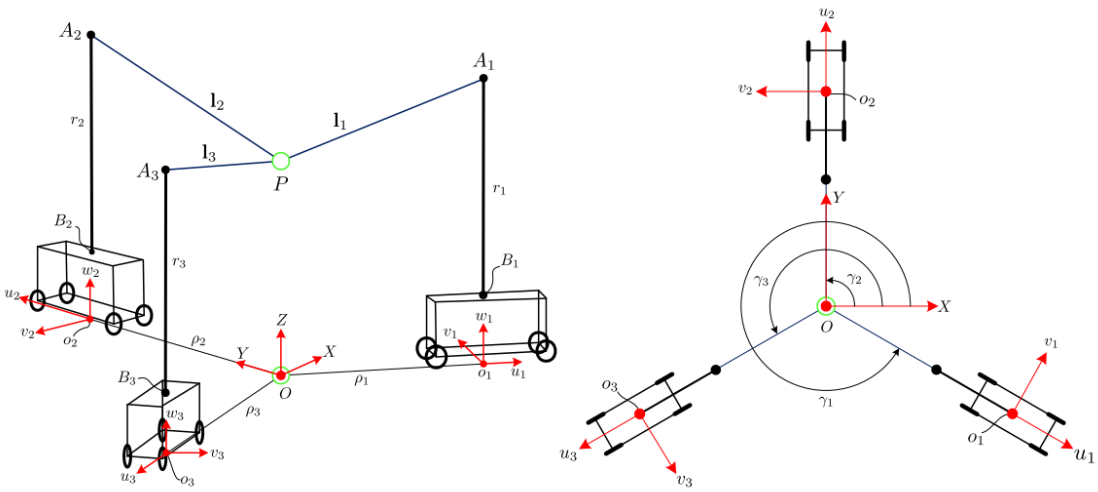

(a) (b)

Figure 3.4 Structure of CDPR on mobile cranes

The end effector is a point mass P of Cartesian coordinate vector $\mathbf{p} = [p_X\ p_Y\ p_Z]^{\mathrm{T}}$. The cables are linked from exit point A_i to point mass P, as shown in Fig 3.4. The exit point A_i is located at the center of the pulley and connected to the lead-screw at point A_i'. The position vector of exit point in fixed coordinate ($\mathcal{F}$) and local coordinate ($\mathcal{L}$) is given by $\mathbf{a}_i^{\mathcal{F}}$ and $\mathbf{a}_i^{\mathcal{L}}$. Vector position of exit point with respect to the local coordinate ($\mathcal{L}$) is written as follows:

$$\mathbf{a}_i^{\mathcal{L}} = \begin{bmatrix} a_i' \\ 0 \\ b_i^z + r_i \end{bmatrix} \tag{3.1}$$

where $a_i' = -0.05m$ is the length from the center of the lead screw (A_i') to the center of the pulley (A_i). The height of the mobile base is stated as b_i^z.

Rotation matrix **R** is needed to transform the value of $\mathcal{L}$ to $\mathcal{F}$. The working rotation matrix is written as follows:

$$\mathbf{R} = \begin{bmatrix} \cos\gamma_i & -\sin\gamma_i & 0 \\ \sin\gamma_i & \cos\gamma_i & 0 \\ 0 & 0 & 1 \end{bmatrix} \tag{3.2}$$

Hence, $\mathrm{a}_\mathrm{i}^{\mathcal{F}} = \left[a_{xi}, a_{yi}, a_{zi}\right]^\mathrm{T}$ is written as follows:

$$\mathbf{a}_i^{\mathcal{F}} = \mathbf{R}\mathbf{a}_i^{\mathcal{L}} = \begin{bmatrix} (\rho_i + a_i')\cos\gamma_i \\ (\rho_i + a_i')\sin\gamma_i \\ b_i^z + r_i \end{bmatrix} \tag{3.3}$$

The crane's length is defined as r_i. The mobile base and crane are connected at point B_i. The position vector of B_i is given as follows:

$$\mathbf{b}_\mathrm{i}^{\mathcal{F}} = \begin{bmatrix} \rho_i.\cos\gamma_i \\ \rho_i.\sin\gamma_i \\ b_i^z \end{bmatrix} \tag{3.4}$$

3.3.2 Trajectory Generation

When performing task, the controller is provided with a steady stream of set points and velocities. This set of specification of the end effector position as a function of time is called trajectory. A fifth order polynomial function of P is used to generate the trajectory of the robot. The path planning of end-effector considers of two segments and each segment consists of two points with three boundary conditions on position, velocity, and acceleration. The fifth order polynomial is determined as follows:

$$\begin{aligned} P_k(t) &= a_k t^5 + b_k t^4 + c_k t^3 + d_k t^2 + e_k t + f_k \\ \dot{P}_k(t) &= 5a_k t^4 + 4b_k t^3 + 3c_k t^2 + 2d_k t + e_k \\ \ddot{P}_k(t) &= 20a_k t^3 + 12b_k t^2 + 6c_k t + 2d_k \end{aligned} \tag{3.5}$$

where $k = 1,2$ represents of each segment. Trajectory will be defined as a function of time, knowing all the parameters of the trajectory v_1, a_1 and position P at initial point P_0, first point P_1, and second point P_2. Note that v_1 and a_1 are the velocity

and acceleration of the end effector. Hence, there are six initial conditions for each segment of the trajectory. The fifth order polynomial is determined as follows:

$$\begin{aligned} p_{1x}(t) &= 2.8 \times 10^{-6}t^5 - 1.54 \times 10^{-4}t^4 + 0.0031t^3 - 0.0277t^2 \\ &\quad + 0.109t - 0.3582 \\ \dot{p}_{1x}(t) &= 1.39 \times 10^{-5}t^4 - 6.18 \times 10^{-4}t^3 + 0.0095t^2 - 0.0556t \\ &\quad + 0.109 \\ \ddot{p}_{1x}(t) &= 5.568 \times 10^{-5}t^3 - 0.0019t^2 + 0.0190t - 0.0556 \end{aligned} \tag{3.6}$$

$$\begin{aligned} p_{1z}(t) &= 3.2 \times 10^{-6}t^5 - 1.7 \times 10^{-4}t^4 + 0.0033t^3 - 0.0284t^2 \\ &\quad + 0.109t - 0.65 \\ \dot{p}_{1z}(t) &= 1.56 \times 10^{-5}t^4 - 6.8 \times 10^{-4}t^3 + 0.0099t^2 - 0.0569t \\ &\quad + 0.109 \\ \ddot{p}_{1z}(t) &= 6.24 \times 10^{-5}t^3 - 0.002t^2 + 0.02t - 0.0569 \end{aligned} \tag{3.7}$$

The second segment which is from point P_1 to P_2 is stated as follows

$$\begin{aligned} p_{2x}(t) &= 2.8 \times 10^{-6}t^5 - 2.63 \times 10^{-4}t^4 + 0.0097t^3 - 0.0174t^2 \\ &\quad + 1.573t - 5.85 \\ \dot{p}_{2x}(t) &= 1.39 \times 10^{-5}t^4 - 0.0011t^3 + 0.0290t^2 - 0.0348t + 1.5735 \\ \ddot{p}_{2x}(t) &= 5.57 \times 10^{-5}t^3 - 0.0032t^2 + 0.058t - 0.3485 \end{aligned} \tag{3.8}$$

$$\begin{aligned} p_{2z}(t) &= -3.2 \times 10^{-6}t^5 + 2.97 \times 10^{-4}t^4 - 0.0011t^3 + 0.195t^2 \\ &\quad - 1.65t + 5.65 \\ \dot{p}_{2z}(t) &= -1.56 \times 10^{-5}t^4 + 0.0012t^3 - 0.033t^2 + 0.388t - 1.654 \\ \ddot{p}_{2z}(t) &= -6.24 \times 10^{-5}t^3 + 0.0036t^2 - 0.0658t - 0.3888 \end{aligned} \tag{3.9}$$

The boundary condition of each segment is stated in the Table 3.3

Table 3.2 Boundary Condition of Given Trajectory

Point	Boundary Condition	X	Y	Z	Unit
P_0	Position	-0.2	0	0.15	m
	Velocity	0	0	0	m/s
	Acceleration	0	0	0.025	m/s^2
P_1	Position	0	0	0.25	m
	Velocity	0.048	0	0	m/s
	Acceleration	0.01	0	0.001	m/s^2
P_2	Position	0.2	0	0.15	m
	Velocity	0	0	0	m/s
	Acceleration	0.001	0	0.001	m/s^2

From the boundary condition, the given trajectory then could be illustrated as shown in Figure 3.5. The end-effector position P_i will then move along the given trajectory as given in Figure 3.5.

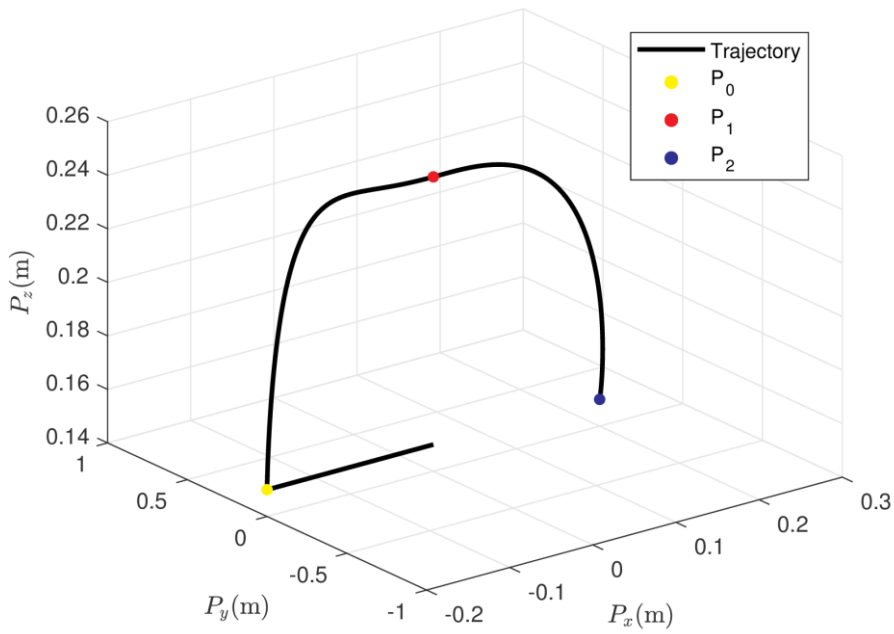

Figure 3.5 Given trajectory for the end-effector

3.3.3 Kinematic Model

The cable vector in fix coordinate is defined as $\mathbf{l}_i^{\mathcal{F}}$, and $i = 1, 2, 3$. Therefore, by using loop closure, the cable vector points from point mass P to exit point A_i can be formulated as follows:

$$\mathbf{l}_i^{\mathcal{F}} = \mathbf{a}_i^{\mathcal{F}} - \mathbf{p} \tag{3.10}$$

The cable length l_i can be defined by the relationship between point mass and exit point. The cable length of the ith cable is as follows:

$$l_i = \|\mathbf{l}_i^{\mathcal{F}}\| = \sqrt{\left(\mathbf{a}_i^{\mathcal{F}} - \mathbf{p}\right)^T \left(\mathbf{a}_i^{\mathcal{F}} - \mathbf{p}\right)}, i = 1,2,3 \tag{3.11}$$

Accordingly, the unit vector of each cable $\mathbf{u}_i^{\mathcal{F}}$ can be computed as follows:

$$\mathbf{u}_i^{\mathcal{F}} = \frac{\mathbf{l}_i^{\mathcal{F}}}{\|\mathbf{l}_i^{\mathcal{F}}\|} \tag{3.12}$$

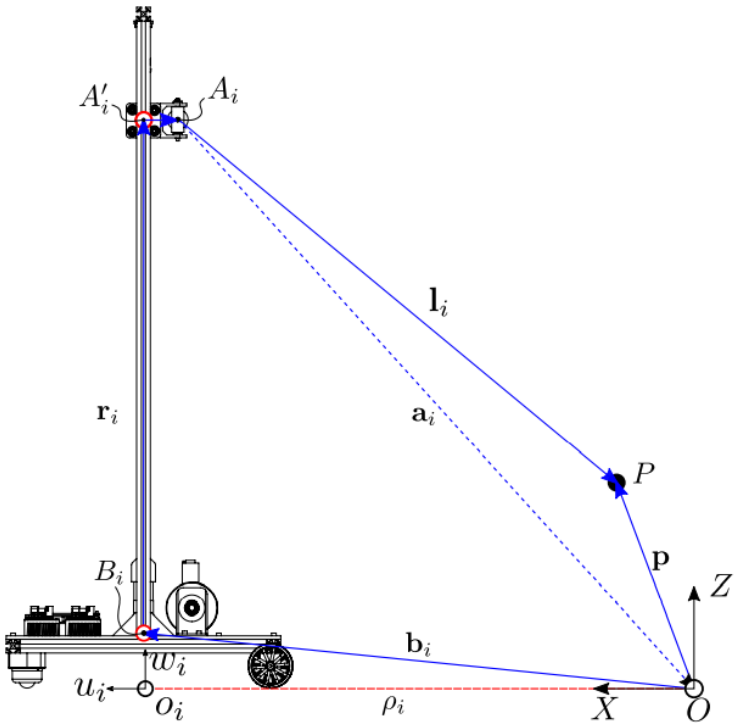

Figure 3.6 Geometric properties of CDPR on mobile crane

The crane length r_i is approached by extending the equation (3.5), as follows:

$$\begin{bmatrix} 0 \\ 0 \\ r_1 + r_2 + r_3 \end{bmatrix} + [\mathbf{u}_1^{\mathcal{F}} \quad \mathbf{u}_2^{\mathcal{F}} \quad \mathbf{u}_3^{\mathcal{F}}] \begin{bmatrix} l_1 \\ l_2 \\ l_3 \end{bmatrix} = \begin{bmatrix} p_x \\ p_y \\ p_z \end{bmatrix} \tag{3.13}$$

By deriving equation (3.7) with respect to time, the following input-output velocity relationship is obtained as follows:

$$\dot{\mathbf{l}} = \mathbf{J}(\dot{\mathbf{p}} - \dot{\mathbf{r}}) \tag{3.14}$$

where $\dot{\mathbf{l}} = \left(\dot{l}_1, \dot{l}_2, \dot{l}_3\right)^{\mathrm{T}}$. **J** is Jacobian matrix which can be mathematically defined as follows:

$$\mathbf{J} = \begin{bmatrix} \mathbf{u}_1^{\mathcal{F}} \\ \mathbf{u}_2^{\mathcal{F}} \\ \mathbf{u}_3^{\mathcal{F}} \end{bmatrix} \tag{3.15}$$

3.3.4 Static Analysis

The CDPR is considered in static equilibrium only when its end-effector and mobile base are all in in static equilibrium. The static analysis is critical to find the zero moment point.

3.3.4.1 Static Analysis of End-Effector

There are 3 mobile bases which are initially placed as shown in Figure 3.4b. The cables are connected from the exit point to end-effector. Figure 3.7 shows the free body diagram of the end-effector at point *P*.

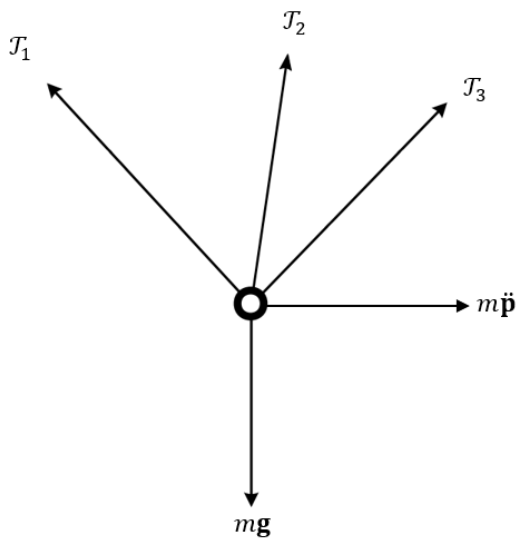

Figure 3.7 Free body diagram of end-effector P

The cables are assumed to be not elastic and the mass is 0. The equation of static equilibrium is expressed as

$$\mathbf{W}\tau + \mathbf{w}_e = 0 \tag{3.16}$$

where $\boldsymbol{\mathcal{T}} = [\mathcal{T}_1 \quad \mathcal{T}_2 \quad \mathcal{T}_3]^{\mathrm{T}}$ is the cables tension vector and $\mathbf{w}_e = [0 \quad 0 \quad -mg]^{\mathrm{T}}$ is the external force which is gravitational force acting at point mass P. The gravity vector is denoted by $\mathbf{g} = [0 \quad 0 \quad -g]^{\mathrm{T}}$ where $g = 9.8\, ms^{-2}$. Since the wrench matrix $\mathbf{W}$ is a square matrix, then the cable tension can be computed as follows:

$$\tau = -\mathbf{W}^{-1}\mathbf{w}_{\mathrm{e}} \tag{3.17}$$

where $\mathbf{W} = \mathbf{J}^{\mathrm{T}}$ and is not singular matrix. Thus, cable force can be computed as follows:

$$\mathbf{f}_{\boldsymbol{i}} = -\mathbf{u}_{\mathrm{i}}^{\boldsymbol{\mathcal{F}}}\tau_i \tag{3.18}$$

Each cable tension is maintained to be positive and greater than $\mathcal{T}_{min} = 1N$ at all time. Hence, the following condition should be fulfilled by Equation:

$$\tau_{min} \leq \tau_i \tag{3.19}$$

3.3.4.2 Static Analysis of The Mobile Base

The mobile crane can only be considered in static equilibrium only when the mobile bases are in fixed position. Figure 3.8 illustrates the free body diagram of the ith mobile crane.

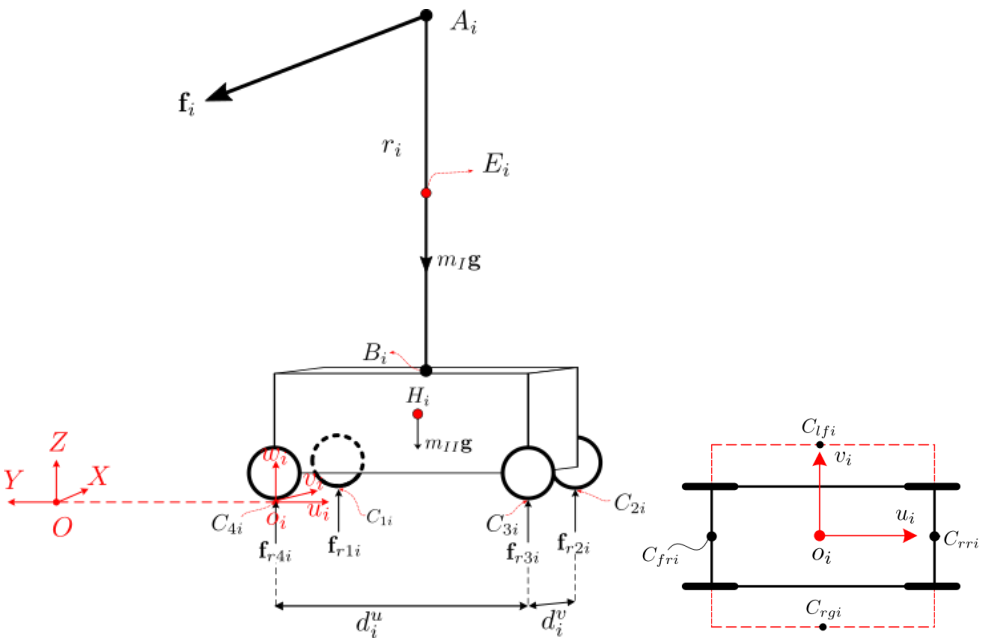

Figure 3.8 Free body diagram of mobile base

The mobile crane is considered to be tipping if it turns over about the v_i axis. The acting frontal and rear reaction forces can be written as follows:

$$\begin{aligned} \mathbf{f}_{fri} &= \mathbf{f}_{r1i} + \mathbf{f}_{r4i} \\ \mathbf{f}_{rri} &= \mathbf{f}_{r2i} + \mathbf{f}_{r3i} \end{aligned} \tag{3.20}$$

By applying Newton's first law of motion, the forces equilibrium is defined as follows:

$$\begin{aligned} \sum \mathbf{f} &= 0 \\ \mathbf{f}_{fri} + \mathbf{f}_{rri} + m_I.\mathrm{g} + m_{II}.\mathbf{g} + \mathbf{f}_i &= 0 \end{aligned} \tag{3.21}$$

And the moment at point O is defined as follows:

.

$$\sum M_O = 0$$
$$\mathbf{c}_{fri} \times \mathbf{f}_{fri} + \mathbf{c}_{rri} \times \mathbf{f}_{rri} + \mathbf{a}_i^{\mathcal{F}} \times \mathbf{f}_i + m_I.\mathbf{e}_i^{\mathcal{F}} \times \mathbf{g} + m_{II}.\mathbf{h}_i^{\mathcal{F}} \times \mathbf{g} = 0 \tag{3.22}$$

where m_I and m_{II} are masses of the crane and mobile base. Their gravitational forces are acting at point E and H. $\mathbf{h}_i^{\mathcal{F}}$ is the position vector of the center of gravity of the mobile base H and $\mathbf{e}_i^{\mathcal{F}}$ is the position vector of the center of gravity of the crane E. $\mathbf{c}_{fri}$ and $\mathbf{c}_{rri}$ are the position vector from the origin O to the front and rear side of the mobile crane as shown in figure 3.6 $\mathbf{c}_{fri}$ and $\mathbf{c}_{rri}$ are defined as follows:

$$\mathbf{c}_{fri} = \begin{bmatrix} \cos(\gamma_i)(\rho_i - L/2) \\ \sin(\gamma_i)(\rho_i - L/2) \\ 0 \end{bmatrix}$$
$$\mathbf{c}_{rri} = \begin{bmatrix} \cos(\gamma_i)(\rho_i + L/2) \\ \sin(\gamma_i)(\rho_i + L/2) \\ 0 \end{bmatrix} \tag{3.23}$$

The vertical components of frontal and rear reactions forces become:

$$f_{rri}^z = m_I g + m_{II} g - f_i^z - f_{fri}^z$$
$$f_{fri}^z = \frac{\left(e_i^y - c_{rri}^y\right).m_I g + \left(h_i^y - c_{rri}^y\right).m_{II} g + \left(c_{rri}^y - a_i^y\right).f_i^z + a_i^z f_i^z}{c_{fri}^y - c_{rri}^y} \tag{3.24}$$

3.3.5 Dynamic Analysis

The dynamic analysis aims to define the behavior of the cable robot when certain amount of forces and moments are imposed onto the moving platform.

3.3.5.1 Dynamic Analysis of The End Effector

The dynamic equilibrium of point P can be derived as

$$\mathbf{W}\tau + \mathbf{w}_e = m\ddot{\mathbf{p}} \tag{3.25}$$

with $\tau = [\tau_1 \quad \tau_2 \quad \tau_3]^{\mathrm{T}}$ acts as the cable tension vector and $\mathbf{w}_e = [0 \quad 0 \quad -mg]^{\mathrm{T}}$ is the gravity. The cable tension can be obtained as

$$\tau = m\mathbf{W}^{-1}(\ddot{\mathbf{p}} - \mathrm{g}) \tag{3.26}$$

The cable force $\mathbf{f}_{\mathrm{i}}$ that applied on the ith cable could be expressed as

$$\mathbf{f}_{\mathrm{i}} = -\mathbf{W}\tau \tag{3.27}$$

3.3.5.2 Dynamic Analysis of The Mobile Base

If the mobile base stumbles upon the axis v_i when executing a given task, the mobile base is considered tipping. Tipping occurs when the magnitude of frontal reaction forces ($\mathbf{f}_{r1i}$ and $\mathbf{f}_{r4i}$) are high and the rear reaction forces ($\mathbf{f}_{r2i}$ and $\mathbf{f}_{r3i}$) are null. The front and rear reaction forces can be defined as

$$\begin{aligned} \mathbf{f}_{fri} &= \mathbf{f}_{r1i} + \mathbf{f}_{r4i} \\ \mathbf{f}_{rri} &= \mathbf{f}_{r2i} + \mathbf{f}_{r3i} \end{aligned} \tag{3.28}$$

The force equilibrium for the whole system can be derived by applying Newton's law of motion as follows:

$$\begin{gathered} \sum \mathbf{f} = m\ddot{\mathbf{p}} \\ \mathbf{f}_{fri} + \mathbf{f}_{rri} + m_I.\mathrm{g} + m_{II}.\mathbf{g} + \mathbf{f}_i = (m_I + m_{II})\ddot{\mathbf{p}} \end{gathered} \tag{3.29}$$

The moment at point O is defined as follows:

$$\begin{gathered} \sum M_O = 0 \\ \mathbf{c}_{fri} \times \mathbf{f}_{fri} + \mathbf{c}_{rri} \times \mathbf{f}_{rri} + \mathbf{a}_i^{\mathcal{F}} \times \mathbf{f}_i + m_I.\mathbf{e}_i^{\mathcal{F}} \times \mathbf{g} + m_{II}.\mathbf{h}_i^{\mathcal{F}} \times \mathrm{g} = 0 \end{gathered} \tag{3.30}$$

3.4 Zero Moment Point (ZMP) of Mobile Base

ZMP is defined as a point within the mobile cranes where the sum of moments due to the front and rear reaction forces are null for tipping. ZMP is computed in the mobile base coordinate ($\mathcal{U}_i, \mathcal{V}_i, \mathcal{W}_i$), therefore, point A_i should be transformed into the mobile base coordinate, as follows:

$$\mathbf{a}_i^{\mathcal{L}} = \begin{bmatrix} a_i^u \\ a_i^v \\ a_i^w \end{bmatrix} = \begin{bmatrix} a_i' \\ 0 \\ b_i^z + r_i \end{bmatrix} \tag{3.31}$$

The cable force expressed in the local coordinate is as follows:

$$\mathbf{f}_i^{\mathcal{L}} = \begin{bmatrix} f_i^u \\ f_i^v \\ f_i^w \end{bmatrix} = \begin{bmatrix} f_i^x \cos(\gamma_i) + f_i^y \sin(\gamma_i) \\ -f_i^x \sin(\gamma_i) + f_i^y \cos(\gamma_i) \\ f_i^z \end{bmatrix} \tag{3.32}$$

3.4.1 ZMP Tipping

ZMP is applied to ensure the mobile crane is in static equilibrium while the end-effector is moving along a given path. The sum of moments at the ZMP can be formulated for tipping analysis as follows:

$$M_{O_i} - \left(\mathbf{f}_{fri} + \mathbf{f}_{rri}\right) \times \mathbf{d}_i = 0 \tag{3.33}$$

d_i is the vector position from the origin o_i to the length and width of the mobile base. The mobile crane will tip about the v_i axis, which means that ZMP will be within the points $C_1 i$ and $C_2 i$ or within the length d_i^u in figure 3.6. Then, equation (3.22) can be extended as follows:

$$d_i^u = \frac{a_i^u f_i^w - a_i^w f_i^u - m_I e_i^u g}{f_{fri}^w + f_{rri}^w} \tag{3.34}$$

3.5 Control Scheme

To perform the desired task, the system will be using the PI controller. Based on the previous research, the robot is using feed-forward plus PI control. The Non-Reconfiguration control scheme is illustrated in Figure 3.9.

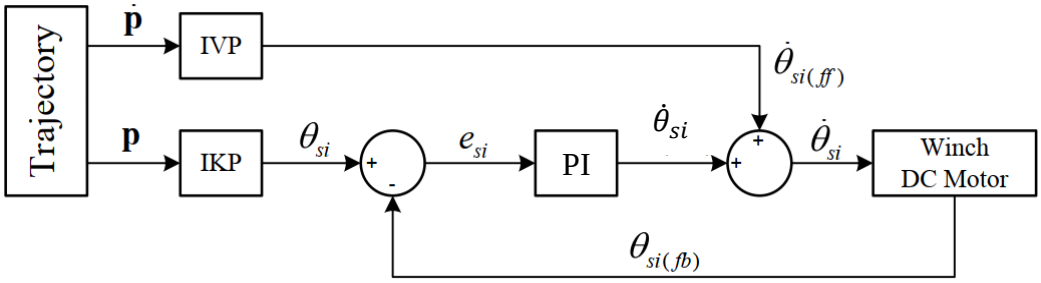

Figure 3.9 The Non-reconfiguration control scheme

- IKP: Inverse Kinematic Problem

The vector **p** and $\dot{\mathbf{p}}$ which are generated from the trajectory generation will be the input of the system. The Inverse Kinematic Problems (IKP) plant has the role to convert the desired trajectory **p** into the associated joint positions $\theta_{si}(t)$. The actuator of the spool and crane are written as follows:

$$\theta_{si} = \frac{l_i}{r_s} \tag{3.35}$$

l_i is as in equation 3.6 θ_{si} and r_s are motor angular position and radius of the spool. The

- IVP: Inverse Velocity Problem

The IVP plant has the role to convert $\dot{\mathbf{p}}$ into $\dot{\theta}_{si}$ which is the motor angular velocity of the spool. $\dot{\theta}_{si}$ can be computed as follows:

$$\dot{\theta}_{si} = \frac{\dot{l}_i}{r_s} \tag{3.36}$$

- PI: Proportional Integral Control

The PI has the role to control the actuators to move along the position which generated in the trajectory generation. The PI controller with additional feed-forward velocity is expressed as follows:

$$\dot{\theta}_{si}(t) = \dot{\theta}_{si(ff)}(t) + K_p e_{si}(t) + K_i \int_0^t e_{si}(t)dt \tag{3.37}$$

$\dot{\theta}_{si(ff)}(t)$ is the angular velocity feed-forward from IVP. $\dot{\theta}_{si}(t)$ is the angular velocity of the actuator or Pulse Width Modulation (PWM) signal for DC Motor. K_p and K_I are the gain to the PI controller.

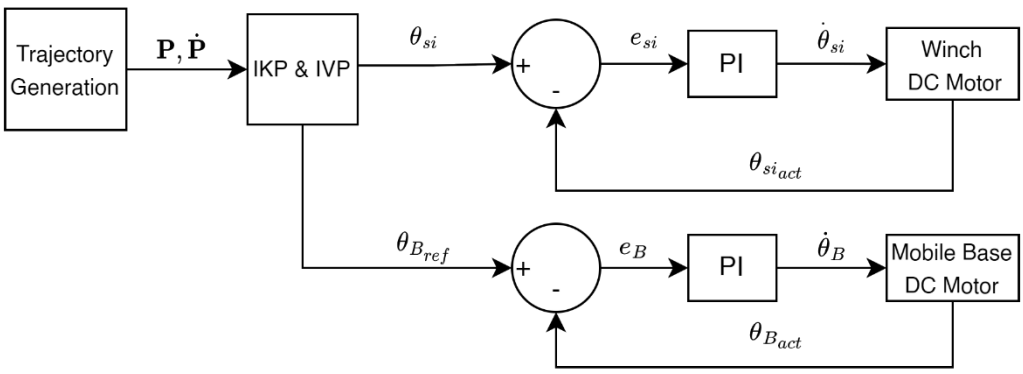

Figure 3.10 Reconfiguration Control Scheme

The PWM is assumed to be linear to the angular velocity of the winch DC motor $\dot{\theta}_{si}$ and mobile base DC motor $\dot{\theta}_B$. The relation between PWM and the angular velocity could be expressed as:

$$\frac{\dot{\theta}_{motor}}{\dot{\theta}_{\max}} = \frac{PWM_{motor}}{PWM_{\max}} \tag{3.38}$$

where $\dot{\theta}_{\max}$ is the maximum angular velocity of the motor, which can be seen in Table 3.4. Since the controller used is a 8-bit microcontroller, then the maximum PWM is 255.

The reconfiguration control scheme is illustrated in Figure 3.10. $\theta_{B_{ref}}$ and $\dot{\theta}_{B_{act}}$ are the angular position and the angular velocity of the actuator or pulse width modulation signal (PWM) input for mobile base DC motor. This control scheme

allows the mobile base move by inputting the distance of the mobile base to the origin ρ_i.

The error of mobile base actuator is denoted as $e_B = \theta_{B_{ref}} - \theta_{B_{act}}$ and $\theta_{B_{act}}$ is respectively the actual angular position and feedback angular position. ρ_i is calculated from the inverse kinematic problem that written as follows:

$$\rho_i = b_i \cos \beta \tag{3.39}$$

β is the angle made between ρ_i and b_i. b_i is the magnitude of the vector $\mathbf{b_i}$ which can be computed from the Equation 3.4.

3.6 PI Tuning

A heuristic tuning method is one where general rules are followed to obtain approximate or qualitative results. The trial-and-error method is an example of heuristic tuning. The trial-and-error method steps through the system from proportional to integral to derivative. This method is a divide and conquer approach, first it puts the system into a rough solution from which small tweaks are performed to perfect the response. It steps through the parameters from proportional to integral to derivative. Usually trial and error starts from an existing set of parameters from which you perform small tweaks to improve the response. For new PI loops trial and error method starts with a rough and safe initial guess.

3.7 Software and Hardware

The robot is using these following software and hardware:

- **Design Software:** SOLIDWORK is a software for 3D CAD design
- **Program Software:** MATLAB/Simulink is selected for program software for the simulation and ARDUINO IDE is used to program the controller.
- **Microcontroller:** ARDUINO DUE which is a micro-controller board based on the Atmel SAM3X8E ARM Cortex-M3 CPU, is selected as a main controller to control the robot.

- **IMU:** Inertia Measurement Unit GY251 IMU is placed on each mobile base for observing the orientation of the mobile base.
- **Motor:** Three types of DC Motors are used as actuators. The specification of each motor is listed in Table 3.4.
  - JGA25-370 is selected as a motor-driven wheel
  - Worm Gear DC Motor is selected for the winch.
  - PG28 DC Motor is used for the crane mechanism

Table 3.3 Motor Specifications

	JGA25-370	**Worm Gear**	**PG28**
Motor Voltage	0-12v	0-12v	0-24v
Gearbox	1:34	1:200	1:52
Speed	126rpm	30rpm	200rpm
Current	46-100mA	60-1700mA	1250mA
Torque	4kg.cm	10kg.cm	15kg.cm

3.8 Comparison of Theoretical and Experimental Results

The error of the end-effector depends on the cable length l_i. The Error of the cable length is computed from the inverse kinematic problem. $l_i(exp)$ is the cable length that is calculated from the rotary encoder of the experiment and l_i is the desired position of the cable length.

By using the range of error principal, the error of cable could be written as follow:

$$\varepsilon_{l_i} = l_i - l_i(exp) \tag{3.40}$$

Table 3.4 Boundary Condition of Maximum Error of Cable Length

Name	$\varepsilon_{l_{min}}[cm] \leq \varepsilon_{l_i} \leq \varepsilon_{l_{max}}[cm]$
Non-Reconfiguration	$-0.6 \leq \varepsilon_{l_i} \leq 0.6$
Reconfiguration Case I and II	$0 \leq \varepsilon_{l_i} \leq 1$

Table 3.4 provides the boundary condition of the maximum error. If the error of cable length stays between the minimum and the maximum error, then the experiment is acceptable. While the boundary condition of the maximum error of mobile base distance to the origin (ρ_i) is listed in Table 3.5

Table 3.5 Boundary Condition of Maximum Error of ρ_i

Name	$\varepsilon_{\rho_{min}}[cm] \leq \varepsilon_{\rho_i} \leq \varepsilon_{\rho_{max}}[cm]$
Reconfiguration Case I and II	$0 \leq \varepsilon_{l_i} \leq 12$

3.8.1 One-Sample t-Test

One-sample t-test compares the mean with a hypothetical value. In this research, the hypothetical values come from the theoretical result. The mean of the theoretical and experimental results of the cable length and ρ will be compared at $t = 5s, 10s, 15s$, and $20s$. The statistical hypotheses could be stated as

$$\mathrm{H}_0: \mu_i = Hypothesized\ \mu$$
$$\mathrm{H}_1: \mu_i \neq Hypothesized\ \mu$$

The significance level used in this research is ($\alpha = 0.05$). The null hypothesis (H_0) will be rejected if P-Value < 0.05 and the alternative hypothesis (H_1) will be accepted.

(This page is empty)

CHAPTER 4
RESULTS AND DISCUSSION

4.1 Wrench Feasible Workspace

Wrench-Feasible Workspace is a set of the end-effector positions that can maintain the static and dynamic equilibrium. The value of cable tension is maintained positive under the external forces. Figure 4.1 shows that the wrench is positive in the workspace as the cable can encounter the force applied onto the end-effector.

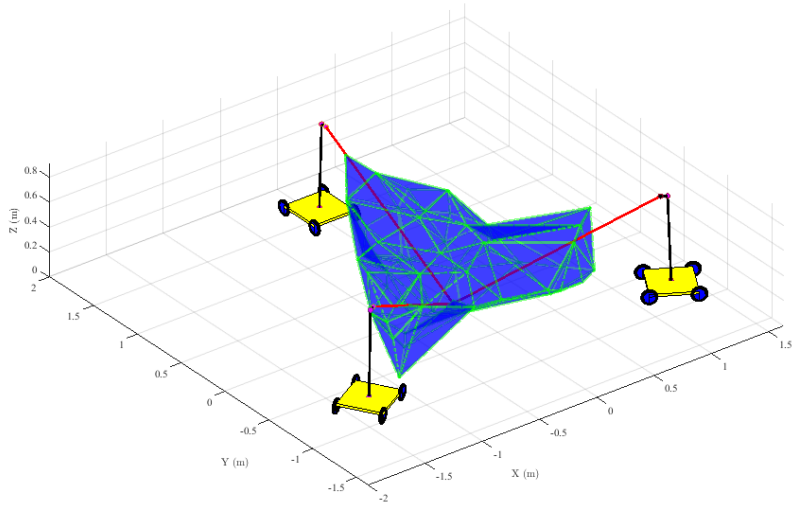

Figure 4.1 Wrench Feasible Workspace

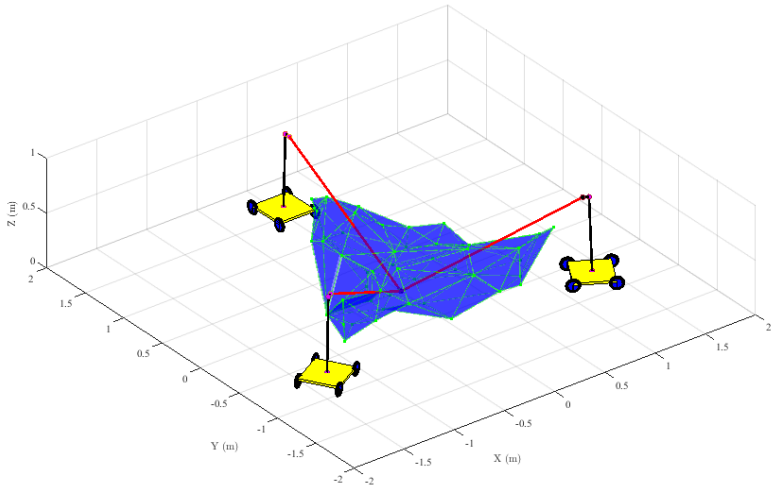

Figure 4.2 Tip-Free Wrench Feasible Workspace

Point P should be located in the tipping-free workspace so that the end-effector can perform a given task. Figure 4.2 shows the tipping-free workspace which has been included the ZMP boundary condition.

4.2 PI Tuning

A heuristic trial and error method is used to tune the PI gains. To start the PI tuning, an existing set of parameters which is provided by previous study (Hor Tan et al., 2021) is used as the initial calibrated gain for the PI controller. The existing gains are shown in Table 4.1.

Table 4.1 Existing Gain

	K_p	K_i
Spool 1	49.5	0.00115
Spool 2	49.5	0.00115
Spool 3	49.5	0.00115
Mobile Base 1	5	0.0001
Mobile Base 2	5	0.0001
Mobile Base 3	5	0.0001

Table 4.1 shiows the provided gains which are then implemented to the microcontroller.. However, the existing gain did not perform well, proved by the high vibration occurred in each motor and the mobile base moved forward more than the desired position. The desired positions of the mobile bases are further explained in Chapter 4.4 and 4.5.

The existing gains are then calibrated by reducing the values of K_p and K_i. The calibrated gains are shown in Table 4.2. By using the calibrated gains, the experimental results are acceptable to validate the theoretical results, proved by the error of cable length and mobile base distance to the origin (ρ_i) are between the lower and upper bound as shown in Table

Table 4.2 Calibrated Gain for Each Motor

	K_p	K_i
Spool 1	35	0.0015
Spool 2	35	0.0015
Spool 3	35	0.0015
Mobile Base 1	0.5	0
Mobile Base 2	0.5	0
Mobile Base 3	0.5	0

4.3 Non-Reconfiguration

In the Non-Reconfiguration case, the end-effector would move along the given trajectory without any mobile base displacement. The payload of 1 kg and 1.3 kg is used in this case. The mobile bases are fixed at 1.5 m from the origin O.

4.3.1 Theoretical Results

With the payload of 1 kg, the end-effector moved along the desired points which generated in the trajectory, as shown in Figure 4.3a. However, the system turns unstable when the payload of 1.3 kg is applied to the end-effector as shown in Figure 4.3b.

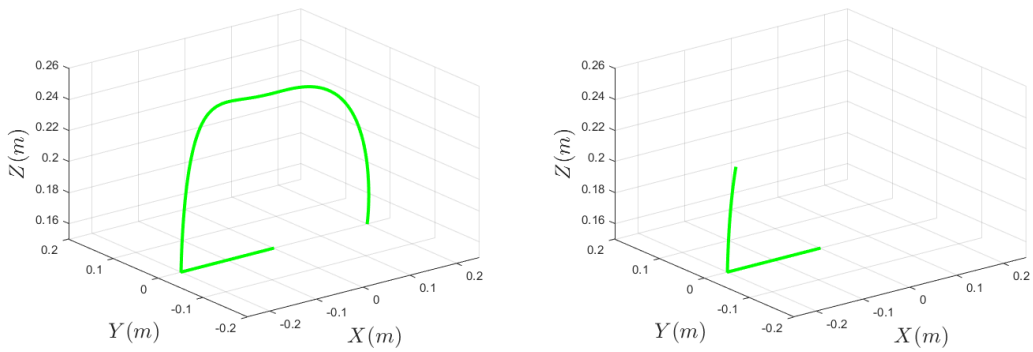

(a) Trajectory Planning of Payload 1kg (b) Trajectory Planning of Payload 1.3kg

Figure 4.3 Non-Reconfiguration Trajectory Planning

Figure 4.3b. shows that the system stopped tracking the end-effector at $t = 7.3s$. Due to the tipping of mobile base, the system did not able to finish the given task. To observe which cable has the highest tension, the data of cable tension with different payload on each cable is presented.

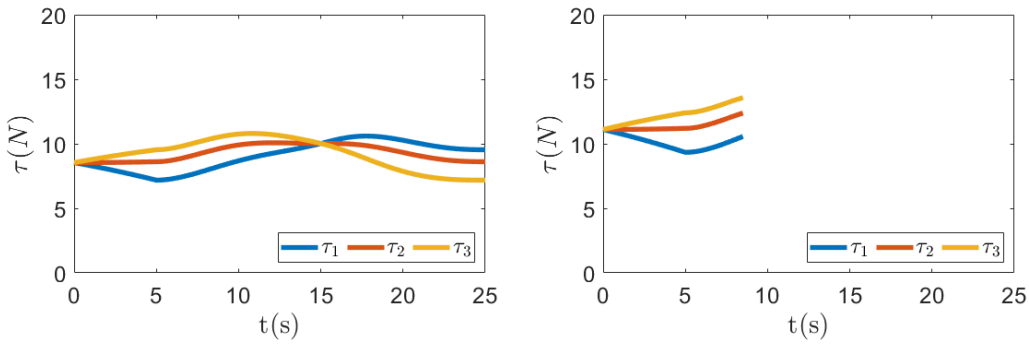

(a) Cable Tension of Payload 1kg (b) Cable Tension of Payload 1.3kg

Figure 4.4 Non-Reconfiguration Cable Tension

For payload 1 kg, the cable tension on each cable of non-reconfiguration case in Figure 4.4 begin at the initial point with similar value. The cable tension on mobile base 3 was the highest at $t = 0 - 15s$. This occurs because the end-effector poses near to the mobile base 3 for the first segment of the trajectory. After 15 seconds, the cable tension of mobile base 1 became the highest due to the end-effector has moved to the second segment of the trajectory which is near to mobile base 1.

Table 4.3 Non-Reconfiguration: Maximum Cable Tension

Cable Tension	Payload 1kg (N)	Payload 1.3kg (N)
τ_1	10.5972	11.1067
τ_2	10.0789	12.3827
τ_3	10.7997	13.5753

As noted in Table 4.3, the theoretical result shows that in non-reconfiguration case with the payload of 1kg, the highest tension is occured on the cable of mobile base 3 with $\tau_3 = 10.7997N$ and the lowest tension is on the cable of mobile base 1 with $\tau_1 = 10.5972N$.

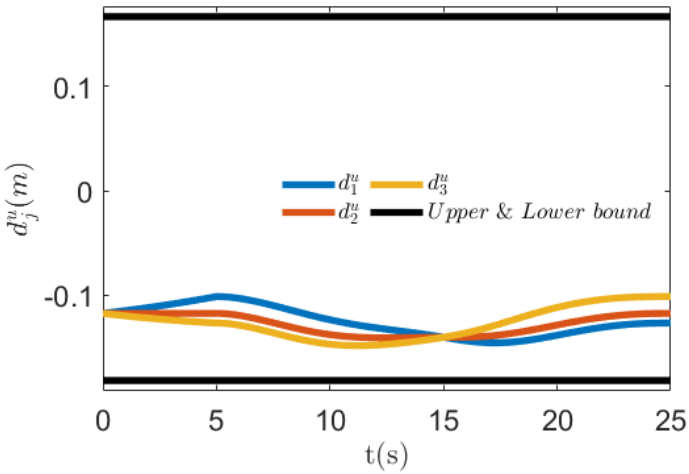

Figure 4.5 ZMP Tipping of Payload 1 kg

Figure 4.5 shows that the d_j^u of each cable in non-reconfiguration with payload 1 kg is still inside the upper and lower bound of ZMP. However, for the non-reconfiguration with payload 1.3 kg, d_3^u has crossed the lower bound at the ZMP at $t = 7.3s$. As there is no displacement of the mobile base, the distance of the mobile base to the origin is maintained the same ($\rho_i = 1.5m$).

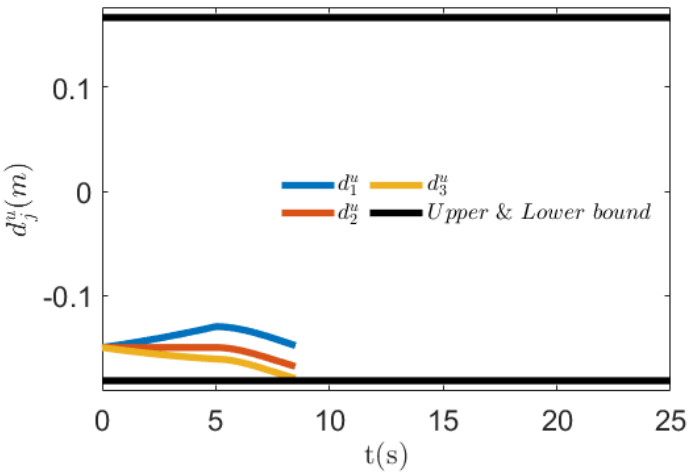

Figure 4.6 ZMP of Payload 1.3 kg

On the other hand, for the payload 1.3 kg, the tracking of cable tension stopped at $t = 7.3s$, as the mobile base tipped and the cable tension $\tau_3 = 13.57N$. As shown in Table 4.1, τ_3 is higher than τ_1 and τ_2.

4.3.2 Experimental Results

The experimental result of non-reconfiguration case with the payload of 1kg is plotted as shown in Figure 4.7. Figure 4.7 depicts the change of cable lengths of each mobile base (l_1, l_2, and l_3) with respective to time (t). The red line represents the actual cable length, while the blue-dashed line is the desired from the theoretical results.

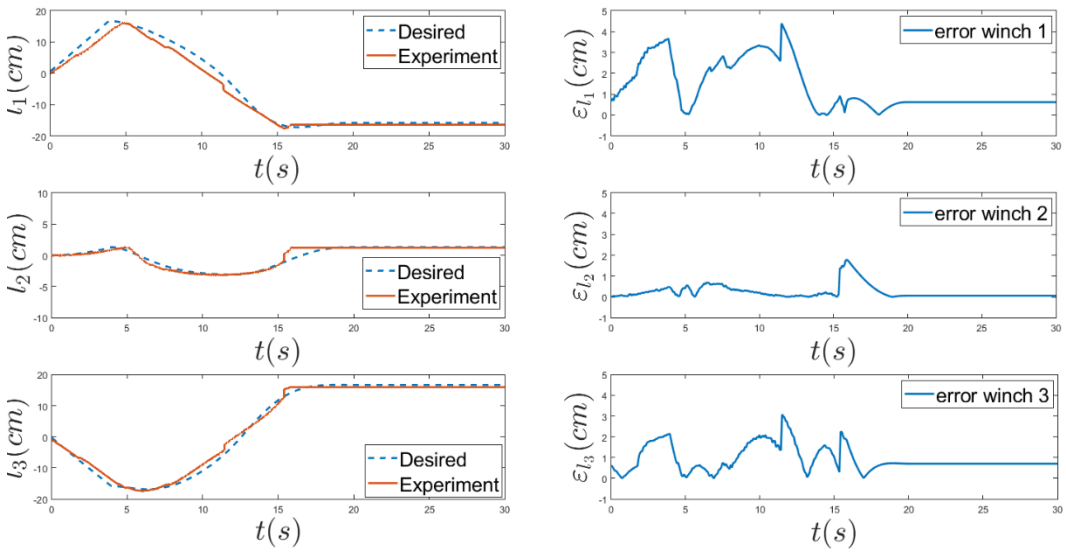

Figure 4.7 Cable Length l_i of payload 1 kg

Figure 4.7 shows that to move the end-effector through the given trajectory, the mobile base 1 uncoiled the cable for 16cm and recoiled for 17.63cm with the maximum error 4.38 cm from the desired. For the mobile base 2, the cable is uncoiled for 1.27cm and recoiled for 3.16cm with the maximum error of 1.775cm from the desired. While the mobile base 3 need to coil the cable first for 17.43cm then uncoiled the cable for 16.03cm with the maximum error of 3.081cm. The error of the experiment result is noted in Table 4.2. The experimental result validates the theoretical result which shows that the cable robot is stable with the payload 1kg.

The experimental result of non-reconfiguration case with the payload of 1.3kg is plotted as shown in Figure 4.8. The red line represents the actual cable length, while the blue-dashed line is the desired from the theoretical results.

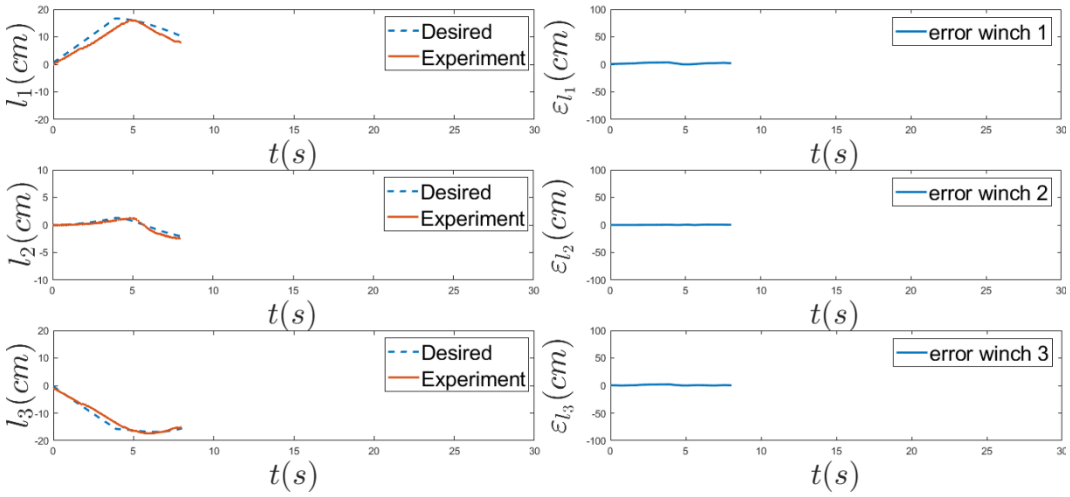

Figure 4.8 Cable Length l_i of Payload 1.3 kg

Figure 4.8 depicts the change of cable lengths of each mobile base (l_1, l_2, and l_3) with respective to time (t). Figure 4.8 shows that to move the end-effector through the given trajectory, the mobile base 1 uncoiled the cable for 16 cm and recoiled for 8cm. For the mobile base 2, the cable is uncoiled for 1.27cm and recoiled for 2.44cm. While the mobile base 3 need to coil the cable first for 17.43cm then uncoiled the cable for 14.98cm until it tipped. The reading stopped at $t = 7.9s$ due to the mobile base 3. The error of the experiment result is noted in Table 4.2. The experimental result validates the theoretical result which shows that the cable robot is unstable with the payload 1.3kg.

Table 4.4 Maximum Error of Cable Length

Cable Length (ε_{l_i})	Payload 1 kg	Payload 1.3 kg
ε_{l_1}	4.3887	3.6619
ε_{l_2}	1.7747	0.6918
ε_{l_3}	3.0815	2.1457

The value of maximum error of the experiment from the desired is listed in Table 4.4. For the non-reconfiguration with the payload of 1kg the cable of mobile base 1(l_1) has the highest maximum error $\epsilon_{l_1} = 4.3887cm$ at $t = 11.48s$. While

for the non-reconfiguration with the payload of 1.3kg, the cable of mobile base 1(l_1) has the highest maximum error $\epsilon_{l_1} = 3.6619cm$ at $t = 3.85s$.

Since both the theoretical and experimental results of the non-reconfiguration case with the payload of 1.3kg shows that the mobile base 3 tipped at 7.9s due to the high tension on the cable, then a reconfiguration is done to reduce the tension τ_i to avoid mobile base 3 from tipping. In this research, the parameters to reconfigure is the distance of the mobile base to the origin O.

4.4 Reconfiguration Case I: Tension Minimization

In Reconfiguration Case I, the objective function is to reduce the cable tensions. The purpose of minimizing the cable tension is to find a set of mobile base position which is defined by ρ_i. The iterative method is used to minimize the tension. The optimization problem can be expressed as follows:

$$\begin{aligned} &minimize : \|\tau\| = \sqrt{\sum_{i=1}^{3}(\tau_i^2)} \\ &\text{over} : \rho_i \in \left[\underline{\rho_i}, \overline{\rho_i}\right] \qquad i \in [1,2,3] \\ &\text{subject to} : \begin{cases} \underline{\tau_i} \leq \tau_i \leq \overline{\tau_i} \\ c_{fri}^u \leq d_i^u \leq c_{fri}^u \end{cases} \end{aligned} \tag{4.1}$$

For the tension minimization, the step of 10cm is for ρ_i with the interval $\rho_i \in [1.1,1.5]$. Each step of ρ_i would check the cable tension whether it is between $\underline{\tau_i} \leq \tau_i \leq \overline{\tau_i}$. Moreover, d_i^u need to be within the upper and lower bounds of ZMP. For reconfiguration case I, the mobile base is allowed to move along the u axis. The maximum and minimum displacement of the mobile base is 1.5m and 1.1m, as shown in Table 4.5.

Table 4.5 Mobile Base Position Reconfiguration Boundary Condition

Parameter	Symbol	Value
Minimum Distance of Mobile Base	$\underline{\rho_l}$	1.1 m
Maximum Distance of Mobile Base	$\overline{\rho_l}$	1.5 m
Maximum Velocity of Mobile Base	$\dot{\rho}$	0.05 m/s
Minimum Cable Tension	$\underline{\tau_l}$	1 N
Maximum Cable Tension	$\overline{\tau_l}$	14 N
ZMP Tipping Upper Limit	c_{rri}^{u}	0.167 m
ZMP Tipping Lower Limit	Cc_{fri}^{u}	-0.180 m

4.4.1 Theoretical Results

With the payload of 1.3 kg, the end-effector moved along the desired points which generated in the trajectory as shown in Figure 4.9. Figure 4.9 shows that the end-effector achieves the desired position of given trajectory without turning over with the reconfiguration. The end-effector has managed to check in each P_i of boundary condition as listed in Table 3.3.

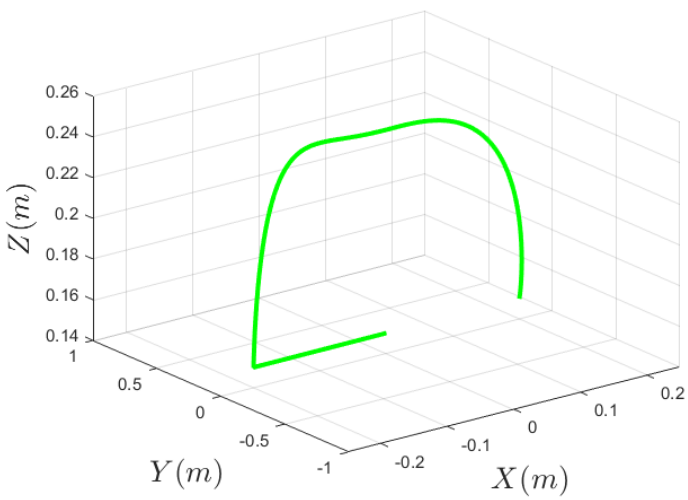

Figure 4.9 Trajectory Planning

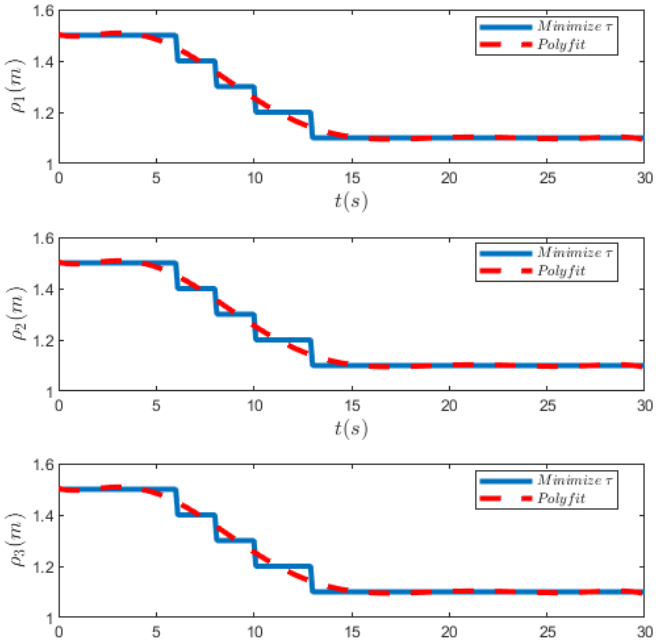

Figure 4.10 The change of ρ of each mobile base

The theoretical results of the mobile base displacement is illustrated in Figure 4.10. The blue line represents the ρ_i with the minimized τ_i and the dashed-red line is the poly-fit which aims to get a smoother result. Figure 4.10 shows the change in the distance of each mobile base to the origin (ρ_i). The mobile bases are discretely moved forward with the step of 10cm.

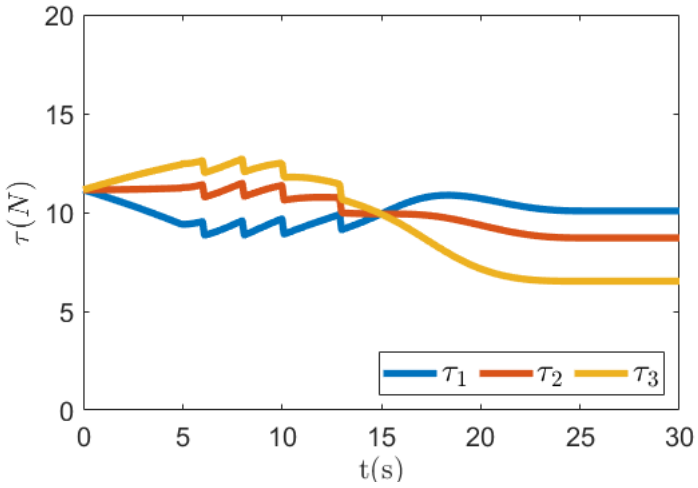

Figure 4.11 Cable Tension on Each Cable

Theoretically, at $t = 6s$, each mobile base should move forward for 40cm, changing the distance of the mobile base to origin from 150cm to 110cm. Figure 4.11 depicts the cable tension on each cable for reconfiguration case I. The maximum cable tension on each cable is listed in Table 4.6.

Table 4.6 Reconfiguration Case I Maximum Cable Tension

Cable Tension	Value (N)
τ_1	11.146
τ_2	11.4866
τ_3	12.7073

Table 4.6 shows that the cable on mobile base 3 is the highest with $\tau_3 = 12.7N$. However, the value of τ_3 is still under the boundary condition $\underline{\tau_i} \leq \tau_i \leq \overline{\tau_i}$, so there is no tipping occurred in reconfiguration case I. The zero moment point analysis validates that the ZMP is still between the upper and lower bound as shown in Figure 4.12.

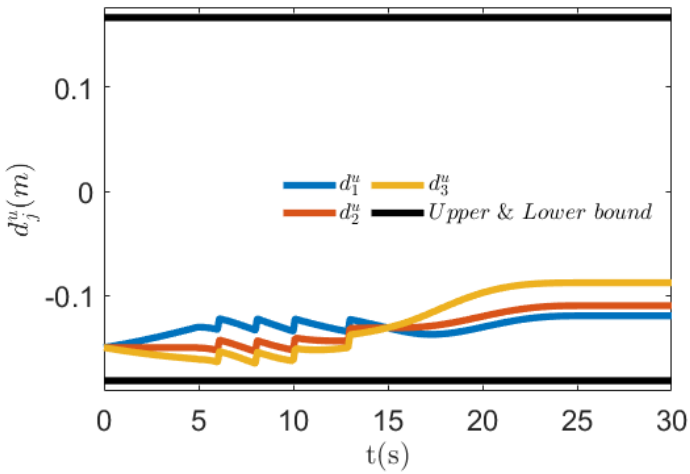

Figure 4.12 ZMP of Reconfiguration Case I

4.4.2 Experimental Results

To validate the simulation results, experiments with the same payload used at the simulation is performed. The experiment is conducted with 3 replicates without changing the configuration in any parameter. Figure 4.13 depicts the change of cable lengths of each mobile base (l_1, l_2, and l_3) with respective to time (t).

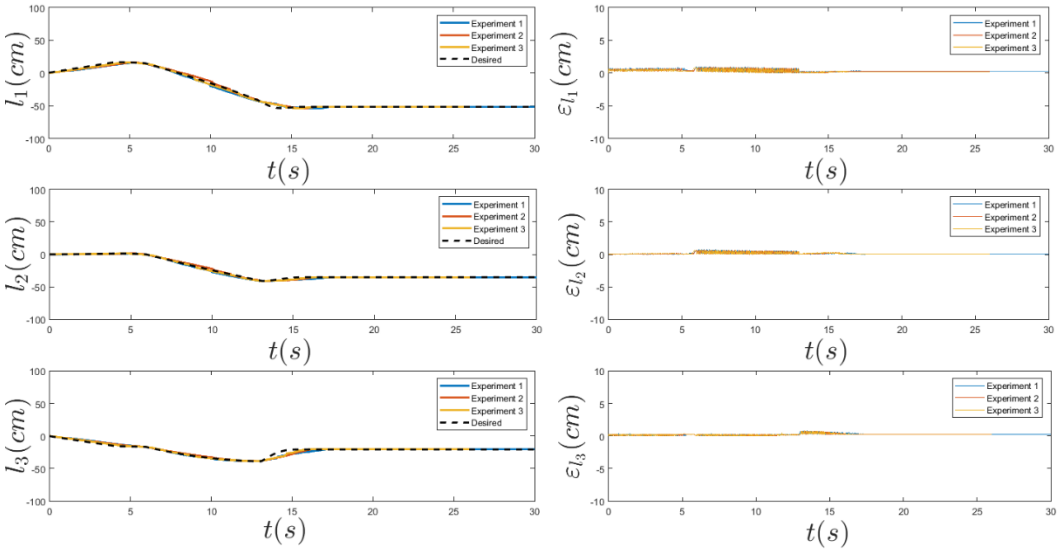

Figure 4.13 Cable Length of Reconfiguration Case I

Figure 4.13 shows that to move the end-effector through the given trajectory, the mobile base 1 uncoiled the cable for 16.33cm and recoiled for 53.92cm on the first run, uncoiling for 16.37cm and recoiling for 53.9cm on the second run and lastly uncoiling 16.43cm and recoiling for 53.86cm on the third run. For the mobile base 2, the cable is uncoiled for 1.29cm and recoiled for 40.97cm on the firt run, uncoiling for 1.33cm and recoiling for 40.92cm on the second run, and uncoiling for 1.36cm and recoiling for 40.91cm on the third run. While the mobile base 3 only coil the cable for 38.74cm on the first run, 38.73cm on the second run, and also 38.73cm on the third run. The maximum error of the experiment result is listed in Table 4.7. The experimental result validates the theoretical result which shows that the cable robot is stable with the payload 1.3kg with reconfiguration case I.

Table 4.7 Reconfiguration Case I: Maximum Error of Cable Length

Cable Length (ε_{l_i})	Experiment 1	Experiment 2	Experiment3
ε_{l_1}	0.9692	0.9103	0.8557
ε_{l_2}	0.7181	0.6770	0.6257
ε_{l_3}	0.7751	0.7519	0.7712

Table 4.7 shows that the maximum error occurred in cable of mobile base 1 which has the highest value with $\epsilon_{l_1} = 0.9692$cm and. Compared to the others, experiment 3 has the lowest cable length error. However, all experimental results of the Reconfiguration Case I are still between the boundary condition.

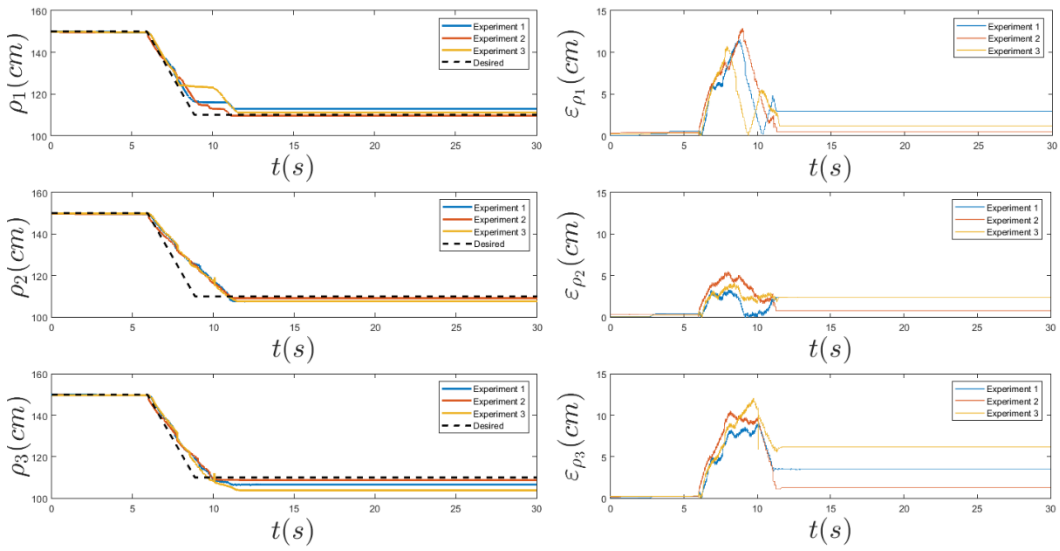

Figure 4.14 Rho in Reconfiguration Case I

Figure 4.14 illustrates the displacement of the mobile base which is represented by the change of the value of ρ_i. For the first run, the mobile base 1 moved 37.02cm forward, moved 40.22cm forward on the second run, and moved 38.6cm forward on the third run. Then on the first run, the mobile base 2 moved 42.35cm forward, moved 40.49cm forward on the second run, and moved 42.29cm forward on the third run. While the mobile base 3 moved 43.6cm forward on the first run, 41,11cm on the second run, and 45.95cm on the third run.

Table 4.8 Reconfiguration Case I: Maximum Error of ρ

ρ (ε_{ρ_i})	Experiment 1	Experiment 2	Experiment3
ε_{ρ_1}	11.5070	12.8711	10.6866
ε_{ρ_2}	3.3039	5.4790	4.0756
ε_{ρ_3}	9.0014	10.5193	12.0553

The difference between the desired and the experiment is noted as error as computed in Equation (3.40). The maximum error of ρ_i is listed in Table 4.8. Table 4.8 indicates that the mobile base 2 has the lowest sum of ϵ_{ρ_2}. On the other hand, mobile base 1 has the highest maximum error on each run. The cable length and ρ from the experiment and theoretical result are then compared by using one-sample t-test and are listed in Table 4.9.

Table 4.9 Reconfiguration Case I: Theoretical and Experimental Results of Cable Length For l_1

t (s)	Theoretical	Experiment 1	Experiment 2	Experiment 3
5	16.152	15.5117	16.1240	16.0213
10	-15.762	-20.0195	-12.7204	-17.8473
15	-52.425	-52.3778	-52.1176	-53.1555
20	-51.585	-51.8858	-51.8329	-51.7843

The statistical hypotheses are:

$$\mathrm{H}_0: \mu_i = -25.9$$

$$\mathrm{H}_1: \mu_i \neq -25.9$$

The hypothesized mean is obtained from the theoretical result which is -25.9. The P-Value obtained from one-sample t-test are shown in Table 4.10.

Table 4.10 Reconfiguration Case I: P-Value from One-Sample t-Test of Cable Length For l_1

Experiment	P-Value
Experiment 1	0.941
Experiment 2	0.966
Experiment 3	0.965

As shown in Table 4.10, all experiments have the P-Value > 0.05, which means the null hypothesis is accepted. With confidence level of 95%, it can be concluded that the experiment results of cable length l_1 are not significantly different, then the experiment results are acceptable to validate the theoretical result. The theoretical and experimental results of l_2, which are being compared, are listed in Table 4.11.

Table 4.11 Reconfiguration Case I: Theoretical and Experimental Results of Cable Length For l_2

t (s)	Theoretical	Experiment 1	Experiment 2	Experiment 3
5	0.876	1.2187	1.3098	0.9804
10	-24.447	-27.3469	-22.1687	-25.8277
15	-35.686	-39.2088	-39.2178	-38.4849
20	-35.167	-35.1988	-35.1713	-35.1275

The statistical hypotheses are:

$$\mathrm{H}_0: \mu_i = -23.61$$

$$\mathrm{H}_1: \mu_i \neq -23.61$$

The hypothesized mean is obtained from the theoretical result which is -23.61. The P-Value obtained from one-sample t-test are shown in Table 4.12.

Table 4.12 Reconfiguration Case I: P-Value from One-Sample t-Test of Cable Length For l_2

Experiment	P-Value
Experiment 1	0.878
Experiment 2	0.984
Experiment 3	0.918

Table 4.12 indicates that all experiments have the P-Value > 0.05, thus the null hypothesis is accepted. With confidence level of 95%, it can be concluded that the experiment results of cable length l_2 are not significantly different from the theoretical result, then the experiment results are acceptable to validate the theoretical result. The theoretical and experimental results of l_3, which are being compared, are shown in Table 4.13.

Table 4.13 Reconfiguration Case I: Theoretical and Experimental Results of Cable Length For l_3

t (s)	Theoretical	Experiment 1	Experiment 2	Experiment 3
5	-16.168	-14.8506	-15.4312	-15.8285
10	-34.027	-35.0549	-32.5958	-34.4458
15	-20.970	-27.3758	-27.7461	-25.7601
20	-20.741	-35.1988	-20.4893	-20.4484

The statistical hypotheses are:

$$\mathrm{H}_0: \mu_i = -22.98$$

$$\mathrm{H}_1: \mu_i \neq -22.98$$

The hypothesized mean is obtained from the theoretical result which is -22.98. The P-Value obtained from one-sample t-test are shown in Table 4.14.

Table 4.14 Reconfiguration Case I: P-Value from One-Sample t-Test of Cable Length For l_3

Experiment	P-Value
Experiment 1	0.362
Experiment 2	0.794
Experiment 3	0.794

As shown in Table 4.14, all experiments have the P-Value > 0.05, then the null hypothesis is accepted. With confidence level of 95%, it can be concluded that the experiment results of cable length l_3 are not significantly different from the theoretical result, then the experiment results are acceptable to validate the theoretical result. For the comparison of ρ_i, the theoretical and experimental data are listed in Table 4.15.

Table 4.15 Reconfiguration Case I: Theoretical and Experimental Results of ρ_1

t (s)	Theoretical	Experiment 1	Experiment 2	Experiment 3
5	150	149.463	149.625	149.684
10	110	115.963	112.919	123.125
15	110	112.941	109.515	111.184
20	110	112.941	109.515	111.184

The statistical hypotheses are:

$$\mathrm{H}_0: \mu_i = 120$$

$$\mathrm{H}_1: \mu_i \neq 120$$

The hypothesized mean is obtained from the theoretical result which is 120. The P-Value obtained from one-sample t-test are shown in Table 4.16.

Table 4.16 Reconfiguration Case I: P-Value from One-Sample t-Test of ρ_1

Experiment	P-Value
Experiment 1	0.772
Experiment 2	0.970
Experiment 3	0.704

Table 4.16 shows that all experiments have the P-Value > 0.05, which means the null hypothesis is accepted. With confidence level of 95%, it can be concluded that the experiment results of ρ_1 are not significantly different from the theoretical result, then the experiment results are acceptable to validate the theoretical result. Then, the theoretical and experimental results of ρ_2, which are being compared, are listed in Table 4.17.

Table 4.17 Reconfiguration Case I: Theoretical and Experimental Results of ρ_2

t (s)	Theoretical	Experiment 1	Experiment 2	Experiment 3
5	150	149.559	149.610	149.779
10	110	117.515	116.309	117.279
15	110	107.581	109.199	107.596
20	110	107.581	109.199	107.596

The statistical hypotheses are:

$$\mathrm{H}_0: \mu_i = 120$$

$$\mathrm{H}_1: \mu_i \neq 120$$

The hypothesized mean is obtained from the theoretical result which is 120. The P-Value obtained from one-sample t-test are shown in Table 4.18.

Table 4.18 Reconfiguration Case I: P-Value from One-Sample t-Test of ρ_2

Experiment	P-Value
Experiment 1	0.857
Experiment 2	0.937
Experiment 3	0.771

Table 4.18 shows that all experiments have the P-Value > 0.05, which means the null hypothesis is accepted. With confidence level of 95%, it can be concluded that the experiment results of ρ_2 are not significantly different from the theoretical result, then the experiment results are acceptable to validate the theoretical result. For the comparison of ρ_3, the data are shown in Table 4.19.

Table 4.19 Reconfiguration Case I: Theoretical and Experimental Results of ρ_3

t (s)	Theoretical	Experiment 1	Experiment 2	Experiment 3
5	150	149.743	149.794	149.765
10	110	108.934	109.265	108.360
15	110	106.507	108.721	103.816
20	110	106.507	108.721	103.816

The statistical hypotheses are:

$$\mathrm{H}_0: \mu_i = 120$$

$$\mathrm{H}_1: \mu_i \neq 120$$

The hypothesized mean is obtained from the theoretical result which is 120. The P-Value obtained from one-sample t-test are shown in Table 4.20.

Table 4.20 Reconfiguration Case I: P-Value from One-Sample t-Test of ρ_3

Experiment	P-Value
Experiment 1	0.857
Experiment 2	0.937
Experiment 3	0.771

Table 4.18 shows that all experiments have the P-Value > 0.05, which means the null hypothesis is accepted. With confidence level of 95%, it can be concluded that the experiment results of ρ_3 are not significantly different from the theoretical result, then the experiment results are acceptable to validate the theoretical result.

4.5 Reconfiguration Case II: ρ Optimization

In Reconfiguration Case I, cable tension τ become the subject to optimize, without optimizing the distance ρ_i, which means the mobile base will move forward to the minimum distance of mobile base $\underline{\rho_i}$ to the origin O. The iterative method is used to minimize the tension is used to minimize the tension. In Reconfiguration Case II, ρ is the subject to optimize in order to avoid the robot from tipping. The optimization problem can be expressed as follows:

$$minimize: \begin{cases} \|\tau\| = \sqrt{\sum_{i=1}^{3}(\tau_i^2)} \\ \|l\| = \sqrt{\sum_{i=1}^{3}(l_i^2)} \end{cases} \tag{4.2}$$

$$\text{over}: \rho_i \in [\underline{\rho_i}, \overline{\rho_i}] \qquad i \in [1,2,3]$$

$$\text{subject to}: \begin{cases} \underline{\tau_i} \leq \tau_i \leq \overline{\tau_i} \\ \underline{\dot{\rho}_i} \leq \dot{\rho}_i \leq \overline{\dot{\rho}_i} \\ c_{fri}^u \leq d_i^u \leq c_{fri}^u \end{cases}$$

For the tension minimization, the step of 10cm is for ρ_i with the interval $\rho_i \in [1.1,1.5]$. Each step of ρ_i would check the cable tension whether it is between $\underline{\tau_i} \leq \tau_i \leq \overline{\tau_i}$. Moreover, d_i^u need to be within the upper and lower bounds of ZMP and the mobile base velocity should be under $\underline{\dot{\rho}_i} \leq \dot{\rho}_i \leq \overline{\dot{\rho}_i}$. For reconfiguration case II, the mobile base is allowed to move along the u axis.

4.5.1 Theoretical Results

The Reconfiguration Case II has managed to stabilize the robot while the end-effector was moving along a given trajectory. In this case, the mobile base moves back-and-forth about the u-axis to reduce the cable tension in each mobile base.

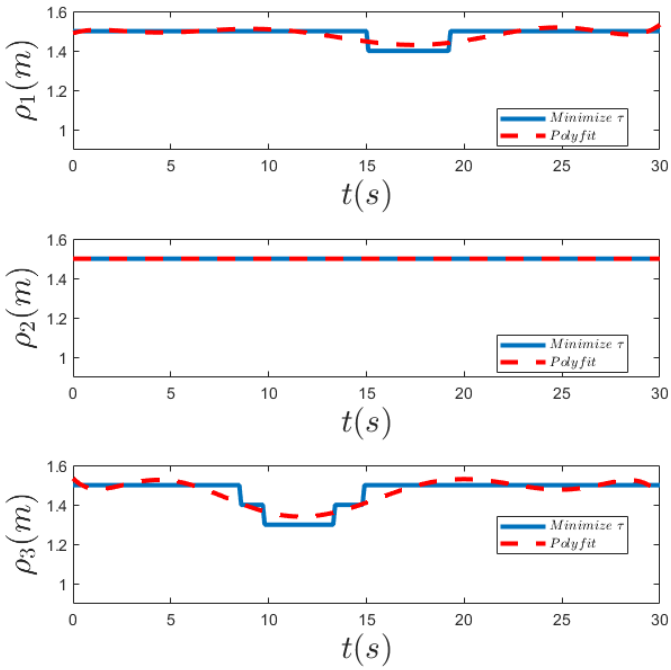

Figure 4.15 ρ value in Reconfiguration Case II

Like in Reconfiguration Case I, the cable tension of mobile base 3 was at the highest for the first 15 seconds, and followed by the mobile base 1 after 15 seconds. In Case II the value of ρ_2 is constant due to the mobile base 2 did not need to reconfigure its position. The value of ρ_3 varies from 1.5-1.3 m and ρ_1 varies from 1.5-1.4 m. This variation shows that the mobile base 1 and 3 were moving forward and backward along the u-axis to reduce the cable tension.

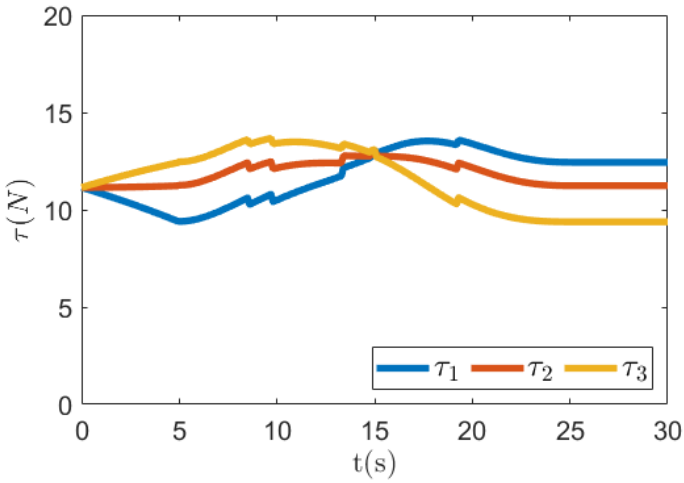

Figure 4.16 Reconfiguration Case II: Cable Tension τ

Figure 4.16 illustrates the cable tension on each cable for Reconfiguration Case II. The theoretical calculation of the maximum cable tension on each mobile base is then listed into Table 4.21.

Table 4.21 Reconfiguration Case II Maximum Cable Tension

Cable Tension	Value (N)
τ_1	13.586
τ_2	13.076
τ_3	13.673

Table 4.21 indicates that the cable on mobile base 3 is the highest with $\tau_3 = 13.673N$. Hence, the value of τ_3 is still under the boundary condition $\underline{\tau_i} \leq \tau_i \leq \overline{\tau_i}$, so there is no tipping occurred in Reconfiguration Case II. The zero moment point analysis validates that the ZMP is still between the upper and lower bound as shown in Figure 4.17.

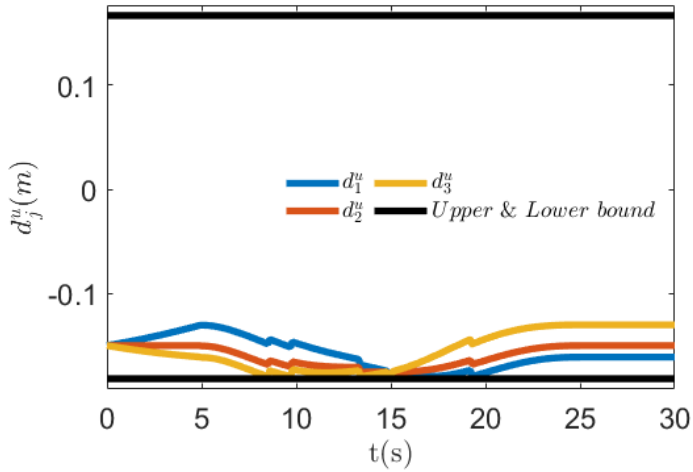

Figure 4.17 ZMP Reconfiguration Case 2

4.5.2 Experimental Results

To validate the simulation results, experiments with the same payload used at the simulation is performed. The experiment is conducted with 3 replicates without changing the configuration in any parameter. Figure 4.18 depicts the change of cable lengths of each mobile base (l_1, l_2, and l_3) in Reconfiguration Case II.

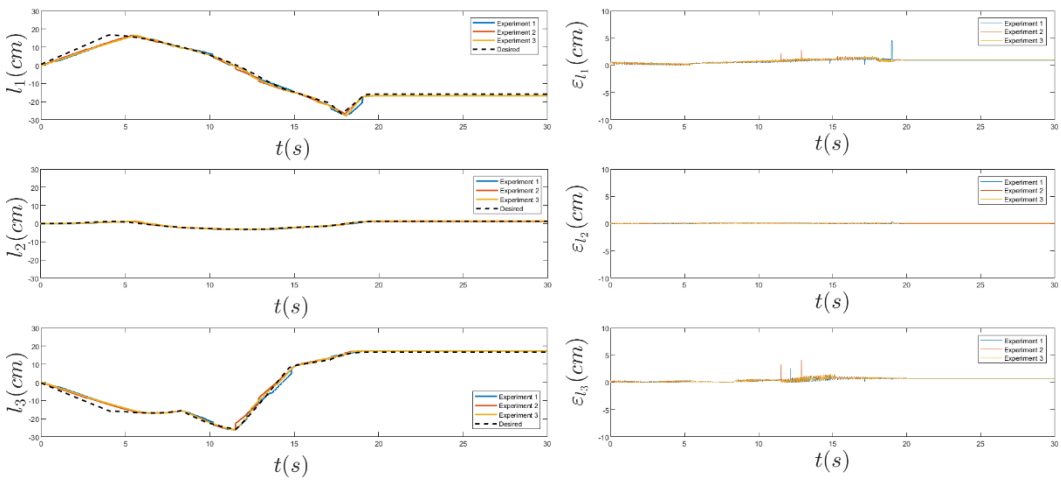

Figure 4.18 Cable Length of Reconfiguration Case II

Figure 4.18 shows that to move the end-effector through the given trajectory, the mobile base 1 uncoiled the cable for 16.48cm and recoiled for 27.75cm on the first run, uncoiling for 16.41cm and recoiling for 26.86cm on the second run and lastly uncoiling 16.43cm and recoiling for 27.77cm on the third run.

For the mobile base 2, the cable is uncoiled for 1.35cm and recoiled for 3.22cm on the firt run, uncoiling for 1.33cm and recoiling for 3.19cm on the second run, and uncoiling for 1.42cm and recoiling for 3.129cm on the third run. While the mobile base 3 firstly coiled the cable for 26.21cm and uncoiled for 17.48cm on the first run, coiled the cable for 26.21cm and uncoiled for 17.5cm on the second run, and coiled the cable for 26.21cm and uncoiled for 17.48cm on the third run. The maximum error of the experiment result is listed in Table 4.22. The experimental result validates the theoretical result which shows that the cable robot is stable lifting the payload 1.3kg with Reconfiguration Case II.

Table 4.22 Maximum Error of cable Length in Reconfiguration Case II

Cable Length (ε_{l_i})	Experiment 1	Experiment 2	Experiment3
ε_{l_1}	0.8377	0.8964	0.8998
ε_{l_2}	0.0699	0.0556	0.0757
ε_{l_3}	0.5592	0.6124	0.6088

Table 4.22 shows that the maximum error occurred in cable of mobile base 1 on the third run with $\epsilon_{l_1} = 0.8998$cm. Experiment 1 has the lowest cable length error. The experimental results of the Reconfiguration Case II are still between the upper and lower bound as described in Table 3.5.

Figure 4.19 illustrates the displacement of the mobile base which is represented by the change of the value of ρ_i. For the first run, the mobile base 1 moved 16.04cm forward at $t = 14.58s$ and back to initial position at $t = 18.9s$, moved 14.65cm forward at $t = 14.8s$ and back to initial position at $t = 18.08s$ on the second run, and moved 15.29cm forward at $t = 14.6s$ and back to initial position at $t = 19s$ on the third run, while the desired is that the mobile base 1 should move 10.04cm forward at $t = 15s$ and back to initial position at $t = 17.5s$.

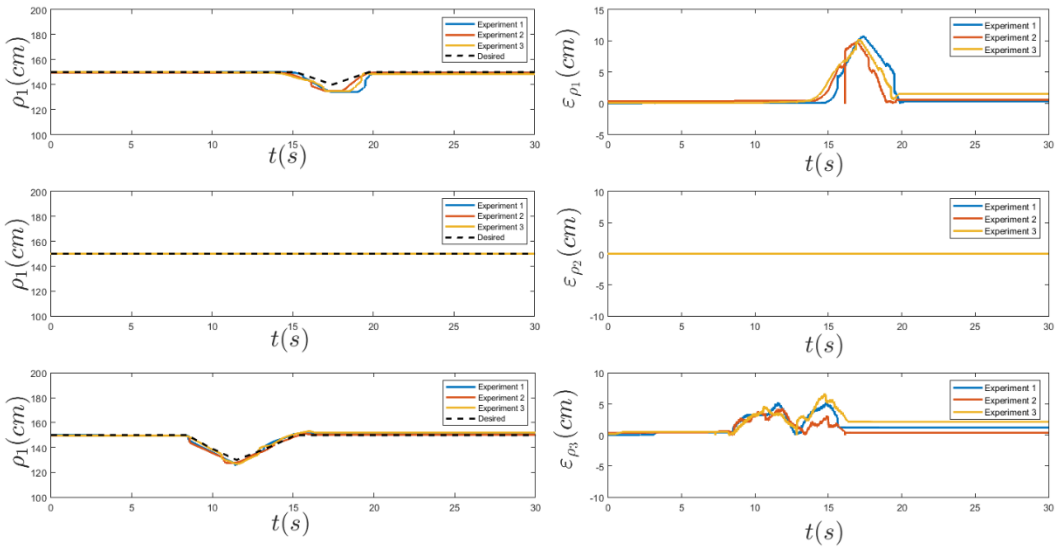

Figure 4.19 ρ in Reconfiguration Case II

The mobile base 2 is remain in the initial position since the desired.indicates that the mobile base 2 did not need to move forward or backward. While for the third mobile base 1 moved 25.45cm forward at $t = 8.5s$ and back to initial position at $t = 11.4s$ on the first run, moved 23.82cm forward at $t = 8.46s$ and back to initial position at $t = 11.26s$ on the second run, and moved 26.5cm forward at $t = 8.46s$ and back to initial position at $t = 11.4s$ on the third run, while the desired is that the mobile base 1 should move 20.284cm forward at $t = 8.5s$ and back to initial position at $t = 11.49s$.

Table 4.23 Maximum Error of ρ

ρ (ε_{ρ_i})	Experiment 1	Experiment 2	Experiment3
ε_{ρ_1}	10.891	9.9359	10.288
ε_{ρ_2}	0.051	0	0.1029
ε_{ρ_3}	5.30	4.3174	6.7224

The difference between the desired and the experiment is noted as error as computed in Equation (3.40). The maximum error of ρ_i is listed in Table 4.23. Experiment 2 has the lowest maximum error. The cable length and ρ from the

experiment and theoretical result of Reconfiguration Case II are then compared by using one-sample t-test and are listed in Table 4.24.

Table 4.24 Reconfiguration Case II: Theoretical and Experimental Results of Cable Length For l_1

t (s)	Theoretical	Experiment 1	Experiment 2	Experiment 3
5	16.067	15.1897	15.4811	14.8336
10	5.400	6.3001	5.5385	5.6218
15	-14.936	-14.9709	-15.0052	-14.9690
20	-15.810	-16.7371	-16.7935	-16.8046

The statistical hypotheses are:

$$\mathrm{H}_0: \mu_i = -2.32$$

$$\mathrm{H}_1: \mu_i \neq -2.32$$

The hypothesized mean is obtained from the theoretical result which is -2.32. The P-Value obtained from one-sample t-test are shown in Table 4.25.

Table 4.25 Reconfiguration Case II: P-Value from One-Sample t-Test of Cable Length l_1

Experiment	P-Value
Experiment 1	0.978
Experiment 2	0.965
Experiment 3	0.952

Table 4.25 shows that all experiments have the P-Value > 0.05, which means the null hypothesis is accepted. With confidence level of 95%, it can be concluded that the experiment results of cable length l_1 are not significantly different from the theoretical result, then the experiment results are acceptable to validate the theoretical result. Then, the theoretical and experimental data of l_2 in Reconfiguration Case II are shown in Table 4.26.

Table 4.26 Reconfiguration Case II: Theoretical and Experimental Results of Cable Length For l_2

t (s)	Theoretical	Experiment 1	Experiment 2	Experiment 3
5	0.809	1.14124	1.16861	1.12822
10	-2.795	-2.73988	-2.79244	-2.70727
15	-2.034	-2.24852	-2.21493	-2.20433
20	1.284	1.27484	1.29318	1.37063

The statistical hypotheses are:

$$\mathrm{H}_0: \mu_i = -0.68$$

$$\mathrm{H}_1: \mu_i \neq -0.68$$

The hypothesized mean is obtained from the theoretical result which is -2.32. The P-Value obtained from one-sample t-test are shown in Table 4.27.

Table 4.27 Reconfiguration Case II: P-Value from One-Sample t-Test of Cable Length l_2

Experiment	P-Value
Experiment 1	0.975
Experiment 2	0.970
Experiment 3	0.948

Table 4.27 indicates that all experiments have the P-Value > 0.05, which means the null hypothesis is accepted. With confidence level of 95%, it can be concluded that the experiment results of cable length l_2 are not significantly different from the theoretical result, then the experiment results are acceptable to validate the theoretical result. The theoretical and experimental data of l_3 in Reconfiguration Case II are listed in Table 4.28.

Table 4.28 Reconfiguration Case II: Theoretical and Experimental Results of Cable Length For l_3

t (s)	Theoretical	Experiment 1	Experiment 2	Experiment 3
5	-16.219	-14.4578	-14.6870	-14.2324
10	-22.647	-21.3021	-22.2348	-22.2244
15	9.313	8.6325	8.7460	8.6819
20	16.685	17.4511	17.4284	17.4387

The statistical hypotheses are:

$$\mathrm{H}_0: \mu_i = -3.22$$

$$\mathrm{H}_1: \mu_i \neq -3.22$$

The hypothesized mean is obtained from the theoretical result which is -3.22. The P-Value obtained from one-sample t-test are shown in Table 4.29.

Table 4.29 Reconfiguration Case II: P-Value from One-Sample t-Test of Cable Length l_3

Experiment	P-Value
Experiment 1	0.936
Experiment 2	0.958
Experiment 3	0.950

Table 4.29 shows that all experiments have the P-Value > 0.05, which means the null hypothesis is accepted. With confidence level of 95%, it can be concluded that the experiment results of cable length l_3 are not significantly different from the theoretical result, then the experiment results are acceptable to validate the theoretical result. For the comparison of ρ_i in Reconfiguration Case II, the theoretical and experimental data are listed in Table 4.30.

Table 4.30 Reconfiguration Case II: Theoretical and Experimental Results of ρ_1

t (s)	Theoretical	Experiment 1	Experiment 2	Experiment 3
5	150.000	149.934	149.662	149.934
10	150.000	149.934	149.603	149.934
15	150.000	149.640	147.794	146.368
20	150.000	149.618	149.419	148.463

The statistical hypotheses are:

$$\mathrm{H}_0: \mu_i = 150$$

$$\mathrm{H}_1: \mu_i \neq 150$$

The hypothesized mean is obtained from the theoretical result which is 150. The P-Value obtained from one-sample t-test are shown in Table 4.31.

Table 4.31 Reconfiguration Case II: P-Value from One-Sample t-Test of ρ_1

Experiment	P-Value
Experiment 1	0.089
Experiment 2	0.142
Experiment 3	0.214

As shown in Table 4.31, all experiments have the P-Value > 0.05, which means the null hypothesis is accepted. With confidence level of 95%, it can be concluded that the experiment results of ρ_1 are not significantly different from the theoretical result, then the experiment results are acceptable to validate the theoretical result. Then, the theoretical and experimental results of ρ_3, which are being compared, are listed in Table 4.32.

Table 4.32 Reconfiguration Case II: Theoretical and Experimental Results of ρ_2

t (s)	Theoretical	Experiment 1	Experiment 2	Experiment 3
5	150	150.000	149.783	149.821
10	150	149.993	149.864	150.000
15	150	149.949	149.574	149.765
20	150	149.949	149.932	149.900

The statistical hypotheses are:

$$\mathrm{H}_0: \mu_i = 150$$

$$\mathrm{H}_1: \mu_i \neq 150$$

The hypothesized mean is obtained from the theoretical result which is 150. The P-Value obtained from one-sample t-test are shown in Table 4.33.

Table 4.33 Reconfiguration Case I: P-Value from One-Sample t-Test of ρ_2

Experiment	P-Value
Experiment 1	0.141
Experiment 2	0.072
Experiment 3	0.086

Table 4.33 shows that all experiments have the P-Value > 0.05, which means the null hypothesis is accepted. With confidence level of 95%, it can be concluded that the experiment results of ρ_2 are not significantly different from the theoretical result, then the experiment results are acceptable to validate the theoretical result. For the comparison of ρ_3, the data are shown in Table 4.34.

Table 4.34 Reconfiguration Case II: Theoretical and Experimental Results of ρ_3

t (s)	Theoretical	Experiment 1	Experiment 2	Experiment 3
5	150.000	149.581	149.574	149.471
10	138.526	136.191	135.449	138.250
15	149.523	150.596	148.294	150.324
20	149.920	151.103	150.265	152.022

The statistical hypotheses are:

$$H_0: \mu_i = 146.9$$

$$H_1: \mu_i \neq 146.9$$

The hypothesized mean is obtained from the theoretical result which is 146.9. The P-Value obtained from one-sample t-test are shown in Table 4.35.

Table 4.35 Reconfiguration Case II: P-Value from One-Sample t-Test of ρ_3

Experiment	P-Value
Experiment 1	0.975
Experiment 2	0.775
Experiment 3	0.877

Table 4.35 shows that all experiments have the P-Value > 0.05, which means the null hypothesis is accepted. With confidence level of 95%, it can be concluded that the experiment results of ρ_3 are not significantly different from the theoretical result, then the experiment results are acceptable to validate the theoretical result.

(This page is empty)

CHAPTER 5
CONCLUSIONS AND FUTURE WORKS

The static and dynamic analysis is performed to get the lower and upper bound of Zero Moment Point of Cable Driven Parallel Robot with three mobile bases. The end-effector is connected to three mobile bases which form a circular formation and separated by 120°. The initial position of the mobile base is set at 1.5 m from the origin and the height of the crane is fixed at 0.68 m. Two study cases of reconfigurations were studied. Both cases have different approaches yet have the same goal, which is reconfigurable mobile base position. PI Controller is used to control the actuator of the CDPR. Trial and error method is used to calibrate the gain needed. The theoretical and experimental results are then compared by using one-sample t-test.

5.1 Conclusions

1. The static and dynamic analysis of CDPR with three mobile bases were presented and discussed. The results of Zero Moment Point analysis represent the static and dynamic equilibrium of the mobile cranes. The ZMP analysis of Reconfiguration Case I and Reconfiguration Case II indicate no tipping occurred in both cases.
2. The robot performance by using PI control has acceptable results, shown by the cable length error and the distance of the mobile base to the origin error are between the boundary condition for both cases. The high error on the ρ experiment is resulted by the motor of the mobile base cannot accurately encounter the cable force.
3. The one-sample t-test shows that all experiments are acceptable to validate the theoretical results. The experiments validate that the end-effector was able to move along the given trajectory on both reconfiguration cases as analyzed in the theoretical results. There is no tipping occurred in the experiment both Reconfiguration Case I and Reconfiguration Case II.

5.2 Future Works

For the future researcher of this topic might want to consider about:

1. The use the cable tension sensor to measure the actual tension on the cable
2. ANN or Genetic Algorithm might be recommended to optimized the study cases.
3. The DC Motor of mobile base could not encounter the cable forces. DC Motors with high torque specification is recommended to use for the mobile base.
4. The vibration analysis needs to be considered to find way to reduce the vibration on the cables.
5. Since IMU is not the best choice for indoor position tracking, camera or sensor like DWM are recommended for tracking the actual end-effector position.
6. XBee module is recommended to use in order to reduce the controller wiring.

REFERENCES

[1.] Albus J., Bostelman R., Dagalakis N. The NIST SPIDER, A robot crane Journal of Research of the National Institute of Standards and Technology, 97 (3) (1992), p. 373

[2.] Pedemonte, N., Rasheed, T., Marquez-Gamez, D., Long, P., Hocquard, É., Babin, F., Fouché, C., Caverot, G., Girin, A., & Caro, S. (2020). FASTKIT: A Mobile Cable-Driven Parallel Robot for Logistics. In *Springer Tracts in Advanced Robotics* (Vol. 132).

[3.] Bostelman, R. v., Albus, J. S., Dagalakis, N., Jacoff, A., & Gross, J. (1994). Applications of the NIST Robocrane. *Robotics and Manufacturing*, *5*.

[4.] Duan, B. Y. (1999). A new design project of the line feed structure for large spherical radio telescope and its nonlinear dynamic analysis. *Mechatronics*, *9*(1), 53–64. https://doi.org/10.1016/S0957-4158(98)00028-2

[5.] Zi, B., Duan, B. Y., Du, J. L., & Bao, H. (2008). Dynamic modeling and active control of a cable-suspended parallel robot. *Mechatronics*, *18*(1), 1–12. https://doi.org/10.1016/j.mechatronics.2007.09.004

[6.] Zi, B., Ding, H., Cao, J., Zhu, Z., & Kecskeméthy, A. (2014). Integrated mechanism design and control for completely restrained hybrid-driven based cable parallel manipulators. *Journal of Intelligent and Robotic Systems: Theory and Applications*, *74*(3–4), 643–661. https://doi.org/10.1007/S10846-013-9848-0

[7.] Alessandro Berti. Kinematics and statics of cable-driven parallel robots by interval-analysis-based methods. Other [cs.OH]. Université Nice Sophia Antipolis, 2015.

[8.] Tahir Rasheed, Philip Long, Stéphane Caro. Wrench-Feasible Workspace of Mobile Cable-Driven Parallel Robots. Journal of Mechanisms and Robotics, American Society of Mechanical Engineers, 2019, pp.1-23.

[9.] H. Tan, L. Nurahmi, B. Pramujati and S. Caro, "On the Reconfiguration of Cable-Driven Parallel Robots with Multiple Mobile Cranes," 2020 5th

International Conference on Robotics and Automation Engineering (ICRAE), 2020, pp. 126-130, doi: 10.1109/ICRAE50850.2020.9310900.

[10.] Syamlan, A.T., Nurahmi, L., Tamara, M.N. *et al.* Dynamic trajectory planning of reconfigurable suspended cable robot. *Int. J. Dynam. Control* **8,** 887–897 (2020).

[11.] Merlet JP (2007) Simulation of discrete-time controlled cable-driven parallel robots on a trajectory. IEEE Trans Robot 33:657–688

[12.] Qian S, Zi B, Shang W-W, Xu Q-S (2018) A review on cable-driven parallel robots. Chin J Mech Eng 31:66

[13.] Gosselin CM (2010) Global planning of dynamically feasible trajectories for three-DOF spatial cable-suspended parallel robots. Mech Mach Sci 12:3–22

[14.] Gagliardini L, Caro S, Goutterfarde M (2015) Optimal path planning and reconfiguration strategy for reconfigurable cable-driven parallel robots

[15.] Gagliardini L, Caro S, Gouttefarde M, Wegner P, Girin A (2014) A reconfigurable cable-driven parallel robot for sandblasting and painting of large structures. In: Cable-driven parallel robots: proceedings of the second international conference on cable-driven parallel robots, pp 275–291

[16.] Hanafie J, Nurahmi L, Caro S, Pramujati B (2018) Design optimization of spatial four cables suspended cable driven parallel robot for rapid life-scan. In: AIP conference proceedings, vol 1983, Article number 060007

[17.] D. Zanotto, G. Rosati, S. Minto and A. Rossi, "Sophia-3: A Semiadaptive Cable-Driven Rehabilitation Device With a Tilting Working Plane," in *IEEE Transactions on Robotics*, vol. 30, no. 4, pp. 974-979, Aug. 2014, doi: 10.1109/TRO.2014.2301532.

[18.] Jin, X., Jung, J., Ko, S.Y., Choi, E., Park, J.O. and Kim, C.S., 2018. Geometric parameter calibration for a cable-driven parallel robot based on a single one-dimensional laser distance sensor measurement and experimental modeling. *Sensors*, *18*(7), p.2392.

[19.] Rosati, G., Zanotto, D. and Agrawal, S.K., 2011. On the design of adaptive cable-driven systems. *Journal of mechanisms and robotics*, *3*(2).

[20.] Nguyen, D.Q. and Gouttefarde, M., 2014, September. Study of reconfigurable suspended cable-driven parallel robots for airplane maintenance. In *2014 IEEE/RSJ International Conference on Intelligent Robots and Systems* (pp. 1682-1689). IEEE.

[21.] Abdolshah, S., Zanotto, D., Rosati, G. and Agrawal, S.K., 2017. Optimizing stiffness and dexterity of planar adaptive cable-driven parallel robots. *Journal of Mechanisms and Robotics*, *9*(3), p.031004.

[22.] Maung, M.M., Latt, M.M. and Nwe, C.M., 2018. DC motor angular position control using PID controller with friction compensation. *International journal of scientific and research publications*, *8*(11), p.149.

AUTHOR BIOGRAPHY

Rizal Muntashir, known as 'Ijal' was born in Surabaya, June 20nd 1997 from the couple of Hidayati Prihartini and Hewin Setyowinarko. His interest in mechatronics began after graduating from SMA Negeri 2 Surabaya, when he went to Politeknik Elektronika Negeri Surabaya in 2015. He started to learn about control system, image processing, and electronics since the second semester in PENS. He had internship at PT. Dirgantara Indonesia in 2018. He assisted the retrofit process of a 5-axis Cincinnati Milling Machine for Aluminium to gain company's efficiency. His final project for the bachelor degree was "Rider less Self-balancing Bicycle", a self-balancing two wheeled vehicle which uses the gyro disc mechanism for the balancing system. He then completed his master program in Department of Mechanical Engineering, Institut Teknologi Sepuluh Nopember in 2022.

For further information, kindly contact the author through:
rizalmuntashir1997@gmail.com